UV Absorption Spectrum of the ClO Dimer (Cl_2O_2) between 200 and 420 nm

Dimitrios K. Papanastasiou,[†,‡] Vassileios C. Papadimitriou,[†,‡,§] David W. Fahey,[†,‡] and James B. Burkholder*[,†]

Earth System Research Laboratory, Chemical Sciences Division, National Oceanic and Atmospheric Administration, 325 Broadway, Boulder, Colorado 80305-3328, and Cooperative Institute for Research in Environmental Sciences, University of Colorado, Boulder, Colorado 80309

Received: July 10, 2009; Revised Manuscript Received: September 28, 2009

The UV photolysis of Cl_2O_2 (dichlorine peroxide) is a key step in the catalytic destruction of polar stratospheric ozone. In this study, the gas-phase UV absorption spectrum of Cl_2O_2 was measured using diode array spectroscopy and absolute cross sections, σ, are reported for the wavelength range 200−420 nm. Pulsed laser photolysis of Cl_2O at 248 nm or Cl_2/Cl_2O mixtures at 351 nm at low temperature (200−228 K) and high pressure (~700 Torr, He) was used to produce ClO radicals and subsequently Cl_2O_2 via the termolecular ClO self-reaction. The Cl_2O_2 spectrum was obtained from spectra recorded following the completion of the gas-phase ClO radical chemistry. The spectral analysis used observed isosbestic points at 271, 312.9, and 408.5 nm combined with reaction stoichiometry and chlorine mass balance to determine the Cl_2O_2 spectrum. The Cl_2O_2 UV absorption spectrum peaks at 244.5 nm with a cross section of $7.6^{+0.8}_{-0.5} \times 10^{-18}$ cm^2 molecule^{-1} where the quoted error limits are 2σ and include estimated systematic errors. The Cl_2O_2 absorption cross sections obtained for wavelengths in the range 300−420 nm are in good agreement with the Cl_2O_2 spectrum reported previously by Burkholder et al. (*J. Phys. Chem. A* **1990**, *94*, 687) and significantly higher than the values reported by Pope et al. (*J. Phys. Chem. A* **2007**, *111*, 4322). A possible explanation for the discrepancy in the Cl_2O_2 cross section values with the Pope et al. study is discussed. Representative, atmospheric photolysis rate coefficients are calculated and a range of uncertainty estimated based on the determination of $\sigma_{Cl_2O_2}(\lambda)$ in this work. Although improvements in our fundamental understanding of the photochemistry of Cl_2O_2 are still desired, this work indicates that major revisions in current atmospheric chemical mechanisms are not required to simulate observed polar ozone depletion.

1. Introduction

Ozone depletion in the Arctic and Antarctic stratosphere during winter and spring is well-established from a variety of satellite, airborne, and ground-based observations.[1] In the Antarctic, ozone depletion is extensive and leads to what is commonly called an "ozone hole". It is recognized that halogen chemistry involving Cl- and Br-containing species is the principal cause of ozone depletion observed in the polar regions.[2] The link between ozone depletion and emission of man-made halogen compounds, e.g., chlorofluorocarbons (CFCs) and bromofluorocarbons (halons), led to the Montreal Protocol and its subsequent amendments and adjustments which regulate global production and consumption of these ozone depleting compounds. Polar ozone depletion alters the composition of Earth's atmosphere and has long-term implications through its impact on climate. Atmospheric models constrained by observations of ozone-depleting compounds predict that the polar and global ozone abundance levels will not return to pre-1980s values (i.e., before the Antarctic stratospheric ozone hole) until later than 2050.[3] Accurate models of current and future atmospheric ozone depletion and recovery require a thorough understanding of the relevant gas-phase and heterogeneous halogen chemistry under the conditions found in the polar regions.

The majority of polar stratospheric ozone loss in current atmospheric model calculations[4] is from the "ClO dimer" catalytic ozone destruction cycle that was first proposed by Molina and Molina[5]

$$ClO + ClO + M \rightarrow Cl_2O_2 + M \quad (1)$$

$$Cl_2O_2 + h\nu \rightarrow Cl + ClOO \quad (2)$$

$$ClOO + M \rightarrow Cl + O_2 + M \quad (3)$$

$$2 \times (Cl + O_3 \rightarrow ClO + O_2) \quad (4)$$

$$\text{NET} \quad 2O_3 + h\nu \rightarrow 3O_2$$

where Cl_2O_2 (dichlorine peroxide, ClOOCl) is referred to as the ClO dimer. A discussion of other catalytic ozone destruction cycles is given elsewhere.[2] Each of the elementary reactions in the ClO dimer cycle has been studied extensively over the last several decades using a variety of laboratory techniques and are considered reasonably well established.[6] Atmospheric model calculations show that in the polar stratosphere the rate of Cl_2O_2 UV photolysis, reaction 2, is critical in determining the rate

* Corresponding author, James.B.Burkholder@noaa.gov.
† Earth System Research Laboratory, Chemical Sciences Division, National Oceanic and Atmospheric Administration.
‡ Cooperative Institute for Research in Environmental Sciences, University of Colorado at Boulder.
§ Current address: Laboratory of Photochemistry and Chemical Kinetics, Department of Chemistry, University of Crete, Vassilika Vouton, 71003, Heraklion, Crete, Greece.

10.1021/jp9065345 CCC: $40.75
Published on Web 11/06/2009

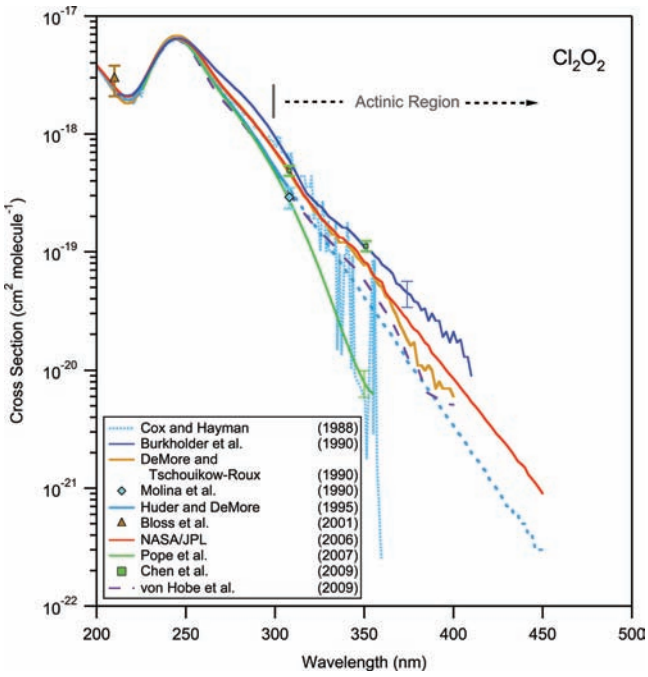

Figure 1. Comparison of Cl_2O_2 UV absorption spectra and cross section values currently available in the literature. The figure illustrates the large scatter in Cl_2O_2 cross section values, particularly in the actinic region. The data for gas-phase Cl_2O_2 spectra recorded at temperatures in the range 195−296 K were taken from Burkholder et al.[9] (blue line), DeMore and Tschuikow-Roux[13] (brown line), Huder and DeMore[16] (light blue line, $\sigma_{Cl_2O_2}(\lambda > 310$ nm) based on extrapolation), Cox and Hayman[15] (dotted line), and Pope et al.[10] (green line). Cross section values at discrete wavelengths are from Bloss et al.[17] (triangle), Molina et al.[7] (diamond), and Chen et al.[19] (squares). The data from Molina et al. and Chen et al. are plotted assuming a Cl_2O_2 photolysis quantum yield of unity. The Cl_2O_2 spectrum in a Ne matrix at 10 K from von Hobe et al.[14] (long dashed line) and the NASA/JPL[6] recommendation (red line) for atmospheric modeling are included for comparison purposes. The earlier studies by Basco and Hunt[24] and Molina and Molina[5] have since been shown[9] to have incorrectly identified the UV spectrum of Cl_2O_2 and are therefore not included.

and extent of ozone depletion. The Cl_2O_2 photolysis rate is determined from the wavelength, λ, dependence of the overlap of its absorption spectrum with the solar flux, which is a function of solar zenith angle, SZA. For photolysis of Cl_2O_2 the most important wavelength region is >300 nm, the actinic region. The photolysis quantum yield for Cl_2O_2 in this wavelength region is thought to be unity although only limited studies are currently available.[7,8] Although UV photolysis of Cl_2O_2 has been clearly shown to be critically important in the ClO dimer catalytic ozone destruction cycle, there exist considerable discrepancies in its UV absorption spectrum, particularly in the most critically important wavelength region. An objective of the present study was to resolve discrepancies in the Cl_2O_2 UV absorption spectrum using laboratory measurements capable of determining the Cl_2O_2 spectrum in this critically important wavelength region.

There are a number of experimental and theoretical studies for the UV absorption spectrum of Cl_2O_2 currently available in the literature including a previous study from our laboratory.[9] A summary of the reported Cl_2O_2 spectra is shown in Figure 1. It is well established that the Cl_2O_2 UV absorption spectrum is continuous with a maximum near 245 nm. However, in the wavelength region λ >300 nm the reported spectra are in poor agreement, which leads to significant levels of uncertainty in the calculated Cl_2O_2 atmospheric photolysis rate. The recent Pope et al.[10] study reported Cl_2O_2 absorption cross sections at λ >300 nm that are significantly lower than those reported in all previous studies. With Cl_2O_2 photolysis rates derived from the Pope et al.[10] spectrum, models produce values of ClO, Cl_2O_2, and ozone and its loss rate that are in poor agreement with in situ and remote-sensing observations.[11] The Pope et al.[10] study, which if correct, would, therefore, have significant implications for the current understanding of halogen chemistry in the polar stratosphere. Furthermore, if Pope et al.[10] were correct, it would mean that the earlier Burkholder et al.[9] study conducted at NOAA was in error outside the stated uncertainty limits. Therefore, an objective of this study was to remeasure the Cl_2O_2 spectrum with a technique that was independent of that used by Burkholder et al.[9]

In this paper, we present a detailed study of the Cl_2O_2 UV absorption spectrum and report absorption cross sections over the wavelength range 200−420 nm. The Cl_2O_2 UV absorption spectrum was measured using complementary experimental techniques and several sources of Cl_2O_2 in order to minimize possible systematic errors. The primary experimental method used was pulsed laser photolysis of Cl_2O or Cl_2O/Cl_2 mixtures, at low temperature and high pressure, to produce ClO radicals and subsequently Cl_2O_2 via reaction 1, combined with diode array spectroscopy. The Cl_2O_2 cross sections obtained in this work at λ >300 nm are in good agreement with the values reported previously by Burkholder et al.,[9] substantially higher than the values reported by Pope et al.,[10] and greater than the values currently recommended by NASA/JPL[6] for use in atmospheric models. This work therefore yields larger Cl_2O_2 atmospheric photolysis rates and more efficient catalytic ozone destruction in the polar stratosphere than those obtained by using the current recommendation. Representative polar stratospheric photolysis rate coefficients, J, are calculated and the uncertainties imposed by the estimated Cl_2O_2 cross section uncertainty are discussed.

2. Experimental Details

The UV absorption spectrum of Cl_2O_2 was determined from data obtained using the apparatus shown in Figure 2. The primary experimental method used pulsed UV laser photolysis (PLP) of gas-phase Cl_2O or Cl_2O/Cl_2 mixtures to produce ClO radicals and subsequently Cl_2O_2 via the termolecular ClO self-reaction, reaction 1, at low temperatures (200−228 K) and high pressure (~700 Torr). Diode array (DA) spectroscopy was used to measure UV absorption spectra of the reaction mixture that contained Cl_2O_2, Cl_2O, and Cl_2 after completion of the ClO radical gas-phase chemistry and the formation of Cl_2O_2. Sequential pulsed photolysis of the sample and the recorded UV absorption spectra were used to deduce the Cl_2O_2 UV absorption spectrum and its absolute cross section values. In the sequence of photolysis steps the partitioning between Cl_2O_2, Cl_2O, and Cl_2 changed while the total chlorine content remained nearly constant (mass balance). Absolute absorption cross sections for Cl_2O_2 were determined at and near the peak of its UV spectrum, 244.5 nm, and other wavelengths in the range 200−420 nm on the basis of three observed isosbestic points, reaction stoichiometry, and chlorine mass balance. (*An isosbestic point is defined as the wavelength where the total absorbance does not change during a chemical reaction.*) A second experimental method employed in this study utilized a cold trapping (CT) technique recently developed by Pope et al.[10] in which bulk Cl_2O_2 samples are collected in the solid phase. Thermal desorption (TD) of the samples containing Cl_2O_2 collected using different trapping temperatures enabled a

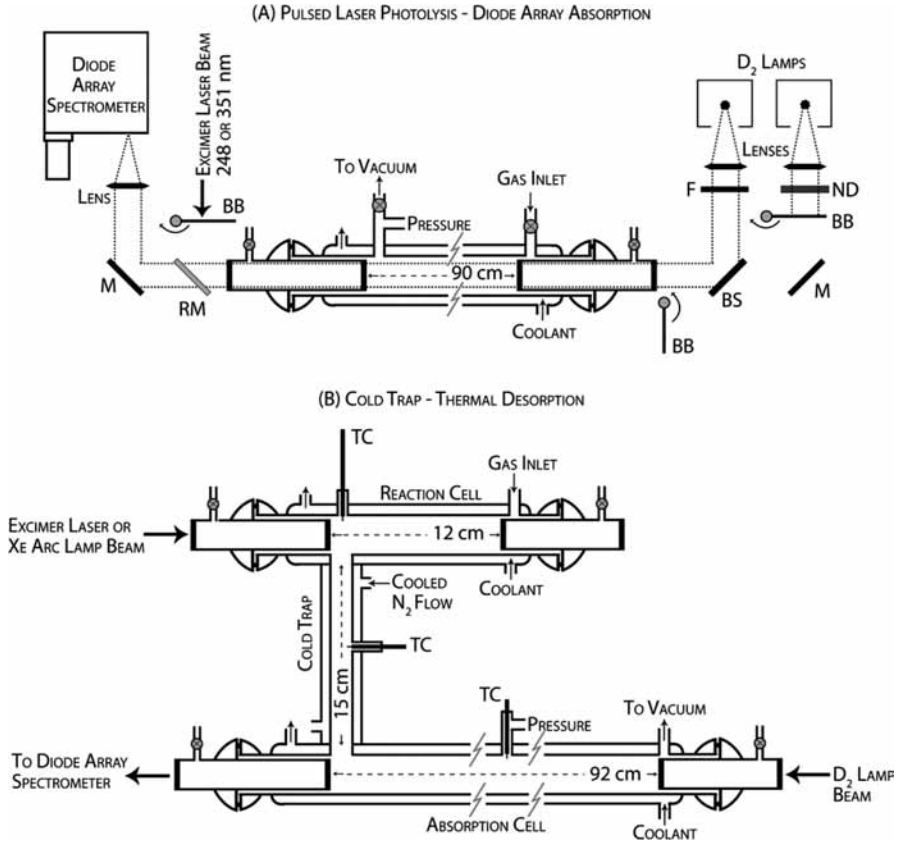

Figure 2. Schematic of experimental apparatus used to study the UV Cl_2O_2 absorption spectrum: (a) pulsed laser photolysis diode array (PLP-DA) setup where M is mirror, RM is a positive position movable dielectric mirror, F is an optical filter, ND is a neutral density filter, BS is a broad band beam splitter, and BB is beam block; (b) cold trap thermal desorption (CT-TD) setup where TC is thermocouple.

qualitative measurement of the Cl_2O_2 absorption spectrum wavelength dependence and an evaluation of the influence of the trapped Cl_2 impurity on the measured spectra. A description of the experimental setups and procedures used in this study is given below.

2.1. Diode Array Spectrometer. UV absorption spectra of gas-phase species were measured by passing a collimated beam from a 30 W D_2 lamp through a temperature-regulated reactor/absorption cell. Two different absorption cells were used as shown in Figure 2 with pathlengths of ~90 cm. The D_2 beam exiting the reactor was focused onto the entrance slit of a 0.5 m spectrometer equipped with a 1024 pixel diode array detector. The spectrometer used an entrance slit width of 150 μm and a 150 grooves mm^{-1} holographic grating. Spectra were measured over the wavelength range 190−530 nm at a resolution of ~1 nm. Emission lines from an Hg pen-ray lamp were used to calibrate the wavelength scale. Typical detector exposure times were 0.3 s, and spectra were obtained from the average of 10 detector readings with a total acquisition time of ~10 s.

Absorption, A, spectra were calculated using Beer−Lambert's law

$$A(\lambda) = -\ln\left(\frac{I(\lambda)}{I_0(\lambda)}\right) = \sum_i (\sigma_i(\lambda) L [x]_i) \qquad \text{(I)}$$

where $I(\lambda)$ and $I_0(\lambda)$ are the measured signals at wavelength λ with and without absorbing species present in the absorption cell, respectively, σ_i is the absorption cross section of species i at wavelength λ, L is the absorption cell path length, and $[x]_i$ is the concentration of species i. The peak-to-peak noise level of an absorption spectrum was typically ~5×10^{-4} absorbance units. Over the duration of an experiment that typically lasted 15 min or less, the drift of the D_2 lamp intensity was <0.001 absorbance units at all wavelengths.

Absorption spectra were measured in pairs using two separate D_2 lamps as shown in Figure 2 to help minimize the influence of second order and scattered light effects. One D_2 lamp was used to measure absorption spectra over the entire wavelength range of the diode array spectrometer, 190−530 nm. For the other D_2 lamp, a long-pass filter was used in the beam path to remove short wavelength radiation and minimize second-order and scattered light effects in the spectrometer. Different combinations of band-pass and long-pass filters were used over the course of our study to confirm the accuracy of the absorption spectra. The majority of the experiments were performed using a WG280 (λ >280 nm) long-pass filter. To improve optical system stability, ease of use, and speed with which spectra were recorded, two separate fixed D_2 lamp setups were used rather than changing optical elements in the beam path during an experiment. The signal intensities from the two lamps were balanced by inserting a neutral density filter in the beam path of the unfiltered lamp. Rapid switching between lamps, a delay of ~1 s, was accomplished using automated beam blocks. Absorption spectra were obtained by combining the two spectra by averaging the signals in the overlapping wavelength region. The agreement in the overlapping wavelength region was always better than 2%.

2.2. Photolysis Sources. An excimer laser operating at 248 (KrF) or 351 (XeF) nm was used as the photolysis source in the pulsed laser photolysis diode array, PLP-DA, experiments, method 1. Laser fluences in the reaction cell were in the range

4−7 mJ cm^{-2} $pulse^{-1}$ for 248 nm and 2−4 mJ cm^{-2} $pulse^{-1}$ for 351 nm as measured with a power meter at the exit of the reactor. The photolysis beam made a single pass through the reactor and nearly filled the reactor volume. For the cold trap thermal desorption, CT-TD, experiments, method 2, the photolysis source was an excimer laser operating at 351 nm, with two passes through the reactor, or a continuous wave 150 W Xe arc lamp. The beam from the Xe arc lamp reflected off a UV cold mirror and passed through a UG5 band-pass filter (220 nm < λ < 430 nm) and a WG320 long-pass filter (λ >320 nm) before entering the photolysis cell. The effective wavelength range used for photolysis was 320−430 nm, and the photolysis beam made a single pass through the reactor. The Xe arc lamp light source was used in the majority of the CT-DT experiments.

2.3. Production of Cl_2O_2. Several chemical schemes were used over the course of the study to produce gas-phase Cl_2O_2. The chemical schemes used different photolytic sources to produce the ClO radical in the gas phase and were used to evaluate the influence of secondary chemistry and spectrally interfering species. All experiments were performed at low temperature (200−228 K) and high pressure (~700 Torr, He) to optimize the production of Cl_2O_2 via reaction 1 and minimize ClO loss via its bimolecular self-reaction

$$ClO + ClO \rightarrow Cl_2 + O_2 \quad (5a)$$

$$\rightarrow ClOO + Cl \quad (5b)$$

$$\rightarrow OClO + Cl \quad (5c)$$

where $k_{5a}(T) = 1.0 \times 10^{-12} \exp(-1590/T)$ cm^3 $molecule^{-1}$ s^{-1}, $k_{5b}(T) = 3.0 \times 10^{-11} \exp(-2450/T)$ cm^3 $molecule^{-1}$ s^{-1}, and $k_{5c}(T) = 3.5 \times 10^{-13} \exp(-1370/T)$ cm^3 $molecule^{-1}$ s^{-1}. (Thermochemical parameters, rate coefficients, quantum yields, and absorption cross section data quoted in this paper are taken from Sander et al.[6] unless noted otherwise.) At the low-temperature and high-pressure conditions used in our experiments reaction 5 was a minor loss for ClO radicals compared to reaction 1 where $k_5/k_1 = 0.0017$ at 200 K and 0.007 at 228 K for 700 Torr (He), k_1(200 K, 700 Torr (He)) = 5×10^{-13} cm^3 $molecule^{-1}$ s^{-1}. At low temperature, the ClO/Cl_2O_2 equilibrium

$$ClO + ClO + M \leftrightarrow Cl_2O_2 + M \quad (1\text{-}1)$$

where $K_c(T) = 9.3 \times 10^{-28} \exp(8835/T)$ cm^3 $molecule^{-1}$ (K_c(228 K) = 6.3×10^{-11} cm^3 $molecule^{-1}$) highly favors the formation of Cl_2O_2 such that the ClO concentration at equilibrium is small (<4×10^{12} molecules cm^{-3}) and below our detection limit in experiments performed at temperatures <210 K.

The ClO radical precursor used in the majority of our 248 nm pulsed photolysis experiments was Cl_2O photolysis

$$Cl_2O + h\nu(248\text{ nm}) \rightarrow Cl + ClO \quad \lambda_T < 843\text{ nm} \quad (6a)$$

$$\rightarrow O + Cl_2 \quad \lambda_T < 713\text{ nm} \quad (6b)$$

$$\rightarrow O + Cl + Cl \quad \lambda_T < 291\text{ nm} \quad (6c)$$

where the photolysis thresholds, λ_T, were calculated using standard heats of formation. Cl_2O absorbs strongly at 248 nm with a cross section of 1.7×10^{-18} cm^2 $molecule^{-1}$ at 298 K and has a photolysis quantum yield of unity. The formation of Cl + ClO is the major product channel and the quantum yield for the formation of Cl atoms has been reported to be >0.9 at 248 nm. The initial Cl_2O concentration was varied over the range $(4.7-7.7) \times 10^{15}$ molecules cm^{-3} and the calculated initial ClO radical concentrations were in the range $(5.6-10.8) \times 10^{13}$ molecules cm^{-3}.

Cl atoms formed in the photolysis of Cl_2O react primarily with Cl_2O following the initial laser pulses of an experiment to form Cl_2 and a ClO radical

$$Cl + Cl_2O \rightarrow Cl_2 + ClO \quad (7)$$

where $k_7(T) = 6.2 \times 10^{-11} \exp(130/T)$ cm^3 $molecule^{-1}$ s^{-1} and k_7(200 K) = 1.2×10^{-10} cm^3 $molecule^{-1}$ s^{-1}. The Cl_2O_2 source chemistry is such that for every two Cl_2O molecules lost there is one Cl_2 and one Cl_2O_2 molecule formed. This stoichiometry leads to the following relationships for the changes in Cl_2O, Cl_2, and Cl_2O_2 concentrations

$$\Delta[Cl_2O] = \Delta[Cl_2] + \Delta[Cl_2O_2] \quad (II)$$

where $\Delta[Cl_2O]$ is defined as $[Cl_2O]_{initial} - [Cl_2O]_{final}$ and

$$\Delta[Cl_2] = \Delta[Cl_2O_2] \quad (III)$$

These stoichiometric relationships are used in the interpretation of the measured UV absorption spectra and determination of Cl_2O_2 absorption cross section values described later. The further photolysis of the reaction mixture leads to a gradual but predictable breakdown of the reaction stoichiometry due to the secondary loss of Cl_2O_2 via photolysis

$$Cl_2O_2 + h\nu(248\text{ nm}) \rightarrow Cl + ClOO \quad (8)$$

where the quantum yield for photolysis is unity and by its reaction with Cl atoms

$$Cl + Cl_2O_2 \rightarrow Cl_2 + ClOO \quad (9)$$

where $k_9(T) = 1 \times 10^{-10}$ cm^3 $molecule^{-1}$ s^{-1}. The ClOO radical formed in reactions 8 and 9 rapidly thermally decomposes

$$ClOO \rightarrow Cl + O_2 \quad (10)$$

where k_{10}(200 K) = 1×10^6 s^{-1} leading to the nearly instantaneous formation of a Cl atom for our experimental conditions. The significance of Cl_2O_2 secondary loss increases as the Cl_2O concentration decreases over the course of an experiment. As a result, the Cl_2O_2 concentration is expected to increase initially and go through a maximum. The Cl_2O photolysis experiments were used to determine the wavelength dependence of the Cl_2O_2 spectrum and its absolute absorption cross sections.

A second source that was extensively used was the 351 nm pulsed laser photolysis of mixtures of Cl_2/Cl_2O. In this method, ClO radical formation was initiated by the photolysis of Cl_2

$$Cl_2 + h\nu(351\text{ nm}) \rightarrow Cl + Cl \quad (11)$$

where the quantum yield for Cl atom production is 2. The initial Cl_2 concentration was in the range $(3-8.3) \times 10^{15}$ molecules cm^{-3} and the initial Cl atom concentrations were $(6-17) \times 10^{12}$ atom cm^{-3} for the range of photolysis laser fluences used. The Cl_2 concentration was kept $<9 \times 10^{15}$ molecules cm^{-3} in order to minimize its initial absorption between 300 and 370 nm. Less than 5% of the initial Cl atom concentration was from Cl_2O photolysis at 351 nm. Cl atoms react with Cl_2O to produce an equimolar amount of ClO. An advantage of this ClO source was that Cl_2O_2 photolysis was significantly reduced due to its smaller absorption cross section at 351 nm compared to 248 nm, the difference in cross section being about a factor of 100. Therefore, higher Cl_2O_2 concentrations were obtained from 351 nm photolysis of Cl_2/Cl_2O than from 248 nm photolysis of Cl_2O. This source was used to determine the wavelength dependence of the Cl_2O_2 spectrum and absorption cross section values.

Another source used to produce ClO radicals was the reaction of Cl atoms with O_3

$$Cl + O_3 \rightarrow ClO + O_2 \qquad (4)$$

where $k_4(T) = 2.3 \times 10^{-11} \exp(-200/T)$ cm^3 $molecule^{-1}$ s^{-1} and the Cl atoms were produced in the 351 nm photolysis of Cl_2. This was the only source used in the CT-TD experiments. In the PLP-DA experiments, the use of high O_3 concentrations interfered with the UV absorption measurements while using low initial O_3 concentrations yielded low Cl_2O_2 concentrations. Therefore, results obtained using this source were primarily limited to determining the wavelength dependence of the Cl_2O_2 absorption spectrum in the wavelength range between 200 and 280 nm.

2.4. Pulsed Laser Photolysis Diode Array Absorption (PLP-DA), Method 1. In this method, the ClO sources described earlier were used to produce Cl_2O_2 in the reactor/absorption cell under static conditions at temperatures in the range 200−228 K. Experiments were primarily performed at high pressure, ∼700 Torr (He), although a few test measurements were performed at lower pressures. The experimental apparatus shown in Figure 2 consists of a temperature-regulated reactor/absorption cell that is optically coupled to the pulsed laser photolysis sources and diode array spectrometer. The photolysis reactor/absorption cell was a jacketed Pyrex tube 105 cm long with an internal diameter of 2.5 cm. The ends of the reactor were sealed with O-ring joint connectors that held two quartz windows separated by an evacuated region, which enabled the entire absorption path to be contained within the temperature-regulated region and prevented condensation on the outside windows. The temperature of the reactor was regulated by circulating methanol from a cooled reservoir through its jacket. The temperature of the reactor was measured at the fluid inlet and outlets and was stable to 0.5 K with a gradient of ∼2 K for a cell temperature of 200 K.

PLP-DA experiments were performed using the following procedure. First, a lamp reference spectrum, I_0, was recorded for both D_2 lamps while flowing He bath gas through the reactor. The reactor was evacuated and filled with reactants while continuously monitoring the contents of the cell by UV absorption. The sample was diluted with He bath gas to a total pressure of >700 Torr (ambient pressure = 623 Torr). The reactant concentrations in the cell were monitored by UV absorption to ensure a well-mixed and homogeneous sample prior to starting photolysis. A spectrum of the sample, I, was recorded for each lamp, and then the photolysis beam steering mirror (RM) was inserted. The sample was then exposed to the photolysis light source. The number of laser pulses used varied depending on the type and conditions of the experiment being performed. The mirror (RM) was then removed, and spectra were recorded for the change in composition of the reactor. This sequence of photolysis and spectrum measurements was then repeated. At the completion of the photolysis experiment, typically after 10−30 photolysis steps, the reactor was flushed out and reference spectra, I_0, recorded again. The total duration of a typical experiment was ∼15 min, although experiments of shorter and longer durations were also performed. The lamp spectra, I_0, measured before and after the sequence of photolysis steps were compared and typically agreed to better than 0.001 absorbance units at all wavelengths. Reference spectra of Cl_2 and OClO were measured immediately following a photolysis experiment at the same temperature and pressure.

2.5. Cold Trap Thermal Desorption (CT-TD), Method 2. The cold trap thermal desorption (CT-TD) apparatus is shown in Figure 2 and was constructed entirely of quartz. The general approach used to study the UV absorption spectrum of Cl_2O_2 with this apparatus follows the methodology developed by Pope et al.[10] to collect bulk samples of Cl_2O_2 and measure its gas-phase absorption spectra during thermal desorption. The three main regions of the apparatus consist of a gas-phase photolysis reactor, a cold trap, and an absorption cell.

The three regions of the apparatus were temperature regulated independently, and the continuity of the temperature-regulated regions helped minimize Cl_2O_2 thermal decomposition during flow through the apparatus. The photolysis reactor was a jacketed 25 cm long cylinder (3 cm i.d.) that was temperature controlled by circulating methanol from a temperature-regulated reservoir through its outer jacket. The temperature of the gas within the reactor was typically 208 K as monitored with a thermocouple inserted in the gas flow (withdrawn during sample preparation). The ends of the reactor were sealed with O-ring joints with quartz windows as described earlier. The cold trap region was a 15 cm long jacketed tube (1.5 cm i.d.) that was temperature-controlled by flowing precooled N_2 gas through its outer jacket. The N_2 gas was cooled by passing it through a copper coil submersed in a liquid N_2 bath. The temperature of the cold trap was regulated between 120 and 155 K by varying the total N_2 flow rate. The temperature of the sample gas flow through the trap region was monitored with a thermocouple located near the center of the trap. Although the temperature of the trap was stable to within 1 K during an experiment, there were significant gradients along its length as measured with a thermocouple inserted along the axis of the gas flow. At 120 K, the difference between the sample gas temperature at the entrance and exit of the trap region was ∼20 K. From here on we will refer to the lowest temperature as the effective temperature of the trap. For sample collection the trap temperature was held constant and independent experiments were performed at various temperatures between 138 and 155 K during our study. The absorption cell had an optical path length of 92 cm, and its temperature was either 200 or 218 K.

The CT-TD experiments were performed by first recording I_0 with only the bath gas flowing (∼15 STP cm^3 s^{-1}, ∼650 Torr) and all regions of the apparatus at ∼200 K. O_3 (0.55−0.65 Torr) and Cl_2 (∼0.22 Torr) were then added to the flow and the sample exposed to the photolysis source while monitoring the formation of Cl_2O_2 and loss of O_3 and Cl_2 in the UV absorption cell. The residence time of the gases in the reactor was ∼6 s. When the absorption signal stabilized, the trap temperature was reduced and a sample collected for ∼90 min. The photolysis source and reactant gas flows were then stopped, the trap temperature was

reduced to ~120 K, and the apparatus was flushed with bath gas. In several experiments the sample was held at 120 K while flushing for ~30 min although this did not significantly affect the absorption results. With the trap at 120 K, there was no detectable absorption in the absorption cell and I_0 was recorded. The trap was then warmed at a rate of ~0.2 K s^{-1} while recording UV absorption spectra of the desorbed sample as it flowed slowly through the absorption cell. During warming, the total bath gas flow was reduced to ~12 STP cm^3 s^{-1} which resulted in a ~50 s residence time for the sample in the absorption cell. In these experiments the D_2 lamp intensity was attenuated to minimize sample photolysis during its residence in the absorption cell.

2.6. Materials. He (UHP, 99.999%), N_2 (UHP, 99.99%), O_2 (UHP, 99.99%), and air (Zero grade) were used as supplied. Cl_2 (UHP grade) mixtures in He or N_2 bath gases were used from commercial sources, 0.2% Cl_2/He (UHP) and 5% Cl_2/N_2 (UHP), or prepared manometrically in a 12 L Pyrex bulb from Cl_2 (UHP, 99.97%), 5.1% Cl_2/He. Ozone was generated by flowing O_2 through an ozonizer and trapped on silica gel at 195 K. Ozone was added to the gas flow by passing a small flow of bath gas through the trap.

Dichlorine oxide (Cl_2O) was prepared by oxidizing Cl_2 with HgO using two methods. Briefly, Cl_2 was condensed at 77 K in a Pyrex reactor containing dried HgO (heated overnight at 400 K) in a Cl_2:HgO mole ratio of ~1:2. The mixture was warmed to 195 K and allowed to stand for 24 h. In the second method, a flow of Cl_2 gas passed through a reactor containing glass beads coated with dry HgO. The gas stream exiting the reactor contained Cl_2O and Cl_2 and was condensed at 195 K. The Cl_2O samples were purified by trap-to-trap distillation to remove the Cl_2 impurity. The Cl_2O purity, >99%, was measured by UV absorption.[6] Cl_2O was added to the apparatus by passing a small flow of bath gas over the liquid sample held in a Pyrex reservoir at 195 K. Reference UV absorption spectra for Cl_2O and Cl_2 were recorded using the diode array spectrometer. The measured Cl_2 spectrum was in excellent agreement with currently recommended values at all temperatures used in this study. For Cl_2O, the temperature dependence of the UV/vis absorption spectrum was not available and was measured in a separate set of experiments. The details of these measurements are given elsewhere.[12]

Chlorine dioxide (OClO) was prepared online by slowly flowing a 5% Cl_2/N_2 mixture through a 25 cm long Pyrex tube containing $NaClO_2$ crystals. The residence time of Cl_2 in the reactor was >60 s, and conversion of Cl_2 to OClO was >95% as determined by UV absorption. $NaClO_2$ crystals were changed frequently to maintain a high OClO production efficiency. Gas flow rates were measured using calibrated electronic mass flow meters. Pressures were measured using a 1000 Torr capacitance manometer.

3. Results and Discussion

Results from the pulsed laser photolysis diode array absorption (PLP-DA) and cold trap thermal desorption (CT-TD) experiments are presented separately below. Analysis of the UV absorption spectra and determination of the wavelength dependence of the Cl_2O_2 UV absorption spectrum and its absolute absorption cross sections follow, and an evaluation of potential errors in the Cl_2O_2 spectrum determination is given. Finally, a brief comparison of the present results with previous studies of the Cl_2O_2 UV absorption spectrum is presented.

3.1. PLP-DA Results. Three photochemical sources were used to produce gas-phase Cl_2O_2 in the reactor/absorption cell under static conditions at reduced temperature. The two Cl_2O_2 sources used in the majority of the experiments utilized the same gas-phase chemistry but were initiated differently. Source 1 used the 248 nm photolysis of Cl_2O and source 2 used the 351 nm photolysis of a Cl_2/Cl_2O mixture to produce ClO radicals. In the third photochemical source, ClO radicals were produced in the Cl + O_3 reaction following 351 nm photolysis of Cl_2 in a Cl_2/O_3 mixture. Although experimental conditions were usually optimized for maximum production of Cl_2O_2, measurements were performed using a range of experimental conditions including variations in temperature, total pressure, photolysis laser fluence, and initial reactant concentrations.

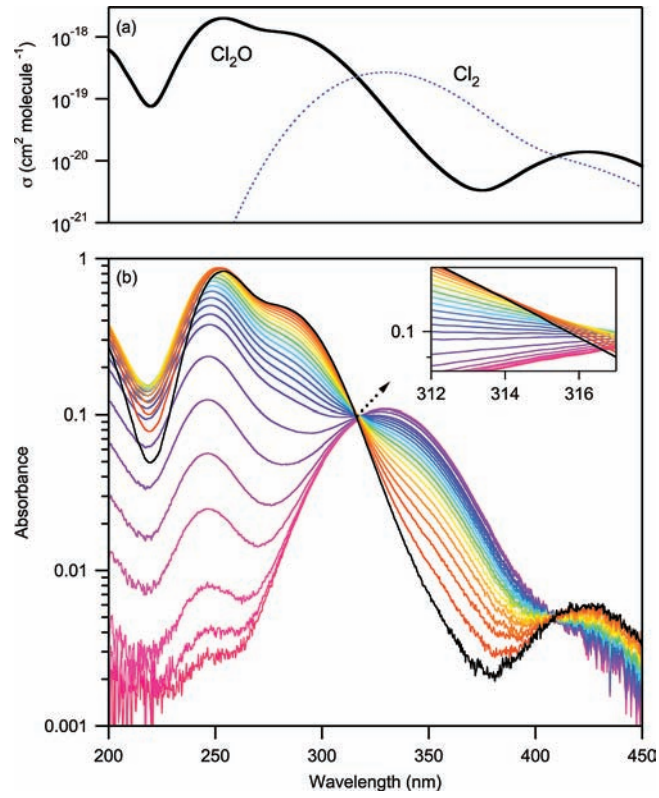

Figure 3. Reference Cl_2O and Cl_2 spectra (frame a) and absorption spectra measured following the pulsed laser photolysis of an initially pure Cl_2O sample at 248 nm (frame b) (see text for details) at 201 K and 725 Torr (He). In frame b the spectrum of the initial Cl_2O sample is shown in black. The additional spectra shown in the figure were obtained following the sequential photolysis of the sample (a static experiment) and show the evolution of the combined absorbance due to Cl_2O, Cl_2, and Cl_2O_2. Spectra were recorded approximately 10 s after each photolysis step (see text for details). The sequence of absorption spectra from the beginning to the end of the experiment is the same as the order of absorbance at 350 nm from low to high values. The initial Cl_2O concentration was 4.7×10^{15} molecules cm^{-3} and the photolysis laser fluence was ~7 mJ cm^{-2} $pulse^{-1}$. The inset shows an expanded view of the isosbestic point observed near 313 nm. An isosbestic point is also observed near 409 nm (see text for details).

Figure 3 shows an example of the UV absorption spectra measured in a 248 nm Cl_2O photolysis, source 1, experiment performed at 201 K and 725 Torr (He). Prior to photolysis the spectrum is due to Cl_2O absorption. The sequence of spectra shown in Figure 3 was recorded following stepwise photolysis of the reactor/absorption cell contents where each spectrum was recorded ~10 s after photolysis. In the initial photolysis steps the gas-phase photochemistry leads to the loss of Cl_2O and production of Cl_2 and Cl_2O_2. This is qualitatively observed in the sequence of spectra by (1) an increase in absorbance in the 330−380 nm region due to the formation of Cl_2 and Cl_2O_2, (2)

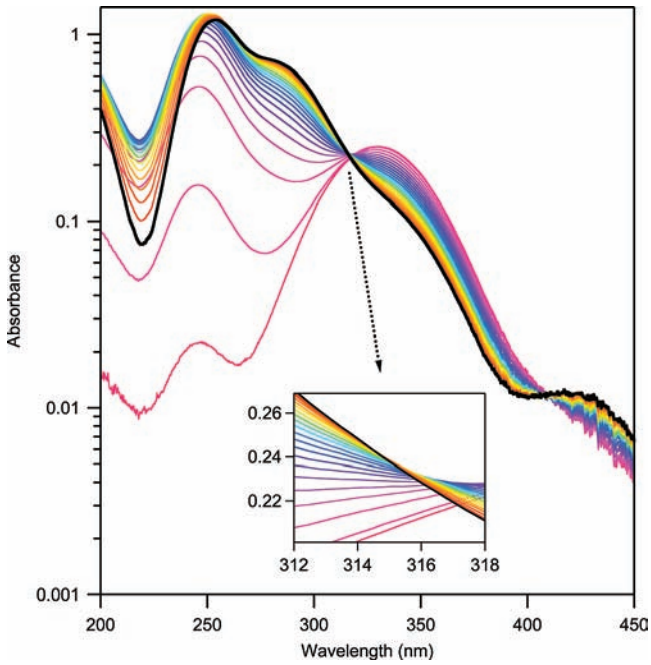

Figure 4. Absorption spectra measured following the pulsed laser photolysis of a Cl_2O/Cl_2 mixture at 351 nm (see text for details) at 201 K and 766 Torr (He). The spectrum of the initial sample is shown in black. The additional spectra shown in the figure were obtained following the sequential photolysis of the sample (a static experiment) and show the evolution of the combined absorbance due to Cl_2O, Cl_2, and Cl_2O_2. Spectra were recorded approximately 10 s after each photolysis step (see text for details). The sequence of absorption spectra from the beginning to the end of the experiment is the same as the order of absorbance at 350 nm from low to high values. The initial concentrations were $[Cl_2O] = 6.8 \times 10^{15}$ molecules cm^{-3} and $[Cl_2] = 4.5 \times 10^{15}$ molecules cm^{-3}, and the photolysis laser fluence was ~3.5 mJ cm^{-2} $pulse^{-1}$. The inset shows an expanded view of the isosbestic point observed near 313 nm. An isosbestic point is also observed near 409 nm (see text for details). The observed isosbestic points are consistent with the results obtained in the 248 nm pulsed photolysis of Cl_2O shown in Figure 3.

a decrease in absorbance at ~280 nm, primarily due to the loss of Cl_2O, and (3) an increase in absorbance near 250 nm and a shift in the absorbance maximum toward shorter wavelengths due to the formation of Cl_2O_2 and loss of Cl_2O. An analysis of the spectra yields the temporal profiles of Cl_2O_2, Cl_2O, and Cl_2 that are presented later.

Figure 4 shows an example of the UV absorption spectra obtained using source 2, 351 nm pulsed laser photolysis of a initial Cl_2O/Cl_2 mixture, at 201 K and a total pressure of 766 Torr (He). The spectra shown are representative of those recorded over the range of experimental conditions used in this study. As observed with source 1, the sequence of UV spectra shows a loss of Cl_2O combined with formation of Cl_2. The Cl_2O_2 concentration goes through a maximum, although higher Cl_2O_2 concentrations were achieved using this source due to the much lower extent of Cl_2O_2 photolysis at 351 nm compared to 248 nm.

PLP-DA experiments performed at temperatures >210 K showed OClO formation that increased with increasing temperature. OClO leads to the formation of Cl_2O_3 via

$$ClO + OClO + M \leftrightarrow Cl_2O_3 + M \qquad (12)$$

and evidence for the formation of Cl_2O_3 was also observed under some conditions. Test experiments were also performed at 200 K and low pressure, ~10 Torr (He). At low pressure the bimolecular ClO + ClO reaction increases relative to the termolecular reaction and leads to the increased formation of OClO via reaction 5c and correspondingly to lower Cl_2O_2 production. The formation of OClO and Cl_2O_3 complicates the determination of Cl_2O_2 absolute absorption cross sections due to uncertainties in the secondary chemistry and spectral analysis. Therefore, only experiments performed at temperatures <210 K and high pressure were included in the final spectral analysis to determine the Cl_2O_2 UV absorption spectrum.

PLP-DA experiments were usually performed with the shortest delay possible between photolysis steps to minimize possible losses of Cl_2O_2. Experiments performed using longer delays, up to 60 s, between photolysis steps, however, yielded very similar results, which indicate that no significant gas-phase chemistry occurred during the time required to measure the UV absorption spectra. Experiments were also performed in which the extent of photolysis per step was altered by varying either the number of photolysis laser pulses or the photolysis laser fluence. The absorption spectra measured using sources 1−3 yielded complementary results and provide the basis for the determination of the wavelength dependence of the Cl_2O_2 UV absorption spectrum and its absolute absorption cross sections described below.

The sequence of UV absorption spectra given in Figures 3 and 4 clearly shows the presence of isosbestic wavelengths near 313 and 409 nm. At these wavelengths, the absorbance remains nearly constant although the concentrations of Cl_2O_2, Cl_2O, and Cl_2 change significantly between photolysis steps. The reaction stoichiometry given in eqs II and III defines a relationship between the absorption cross sections for Cl_2O_2, Cl_2O, and Cl_2 at the isosbestic wavelength

$$\sigma_{Cl_2O_2}(\lambda_{iso}, T) = 2\sigma_{Cl_2O}(\lambda_{iso}, T) - \sigma_{Cl_2}(\lambda_{iso}, T) \qquad (IV)$$

where λ_{iso} is the isosbestic wavelength and $\sigma_{Cl_2O}(\lambda_{iso},T)$ and $\sigma_{Cl_2}(\lambda_{iso},T)$ are the absorption cross sections for Cl_2O and Cl_2, respectively, at λ_{iso} and temperature T. This relationship provides a method to directly determine the Cl_2O_2 absorption cross section at the isosbestic wavelengths from the Cl_2 and Cl_2O absorption cross sections at the same wavelength. Although sources 1 and 2 initiate the Cl_2O_2 formation chemistry differently, the reaction stoichiometry for these two sources is the same. Therefore, the isosbestic points are expected to be the same for both sources as was observed. Note that the observation of an isosbestic point at 408.5 nm provides direct evidence that Cl_2O_2 absorbs in this wavelength region.

For perspective, we note that isosbestic points would have been predicted, for the $Cl_2O_2/Cl_2O/Cl_2$ reaction system even if Cl_2O_2 did not absorb between 200 and 450 nm. However, in that case the isosbestic points would have fallen at ~322 and ~400 nm (for experiments performed at 200 K). The isosbestic wavelengths observed here are significantly shifted from these values indicating that Cl_2O_2 absorbs at these wavelengths.

Upon close examination, the isosbestic point observed near 313 nm is not strictly constant but shifts gradually toward longer wavelengths during the course of an experiment as shown in the insets in Figures 3 and 4. The shift toward longer wavelength is consistent with the breakdown of the reaction stoichiometry due to the loss of Cl_2O_2 via secondary chemistry, photolysis, and reaction with Cl atoms. The breakdown in stoichiometry is systematic and predictable with the shift toward longer wavelength resulting from the fact that the Cl_2O_2 absorption cross

section at this wavelength is greater than that of Cl_2. A more detailed analysis of the systematic dependence of the isosbestic point shift and the dependence on the Cl_2O_2 absorption cross section is given in the Supporting Information. A systematic shift in the 408.5 nm isosbestic point was not observed within the measurement uncertainty because the Cl_2O_2 absorption cross section is similar in magnitude to those of Cl_2O and Cl_2 at this wavelength.

The observed isosbestic wavelengths were found to be independent of temperature (200−228 K), the initial concentrations of Cl_2 and Cl_2O, and addition of O_2 (10 Torr) to the reaction mixture. Experiments performed using band-pass (309 nm, fwhm = 10 nm) and cutoff optical filters (WG-320 (λ >320 nm) and WG-375 (λ >375 nm) to isolate the isosbestic wavelength regions yielded identical results. The 408.5 nm isosbestic point was also examined in an experiment with a higher Cl_2O_2 concentration (a factor of ~4) than that shown in Figures 3 and 4. In this measurement absorption at wavelengths <300 nm was optically thick. However, the signal in the long wavelength region was greater and thereby enabled a more accurate absorption measurement. The isosbestic wavelength was identical to that observed in the lower concentration experiments, and no significant shift in the isosbestic wavelength with extent of reaction was observed which is consistent with a Cl_2O_2 cross section that is similar in magnitude to that of Cl_2 and Cl_2O at 408.5 nm.

The isosbestic wavelength in the limit of zero concentration change was determined in the source 1 experiments to be 312.9 ± 0.16 where the quoted uncertainty is the standard deviation of seven measurements. The isosbestic wavelength determined using source 2 was consistent with the source 1 results although the precision in nine measurements was lower, ±0.69 nm. In addition to the isosbestic points observed at 312.9 and 408.5 nm, a pseudoisosbestic point was observed near 271 nm at low Cl_2O conversion. In an earlier study, DeMore and Tschuikow-Roux[13] reported an isosbestic point at 271 nm in their Cl_2/Cl_2O photolysis experiments. In our experiments, the behavior of the absorbance near 271 nm was very sensitive to Cl_2O_2 loss and the breakdown of the reaction stoichiometry. This sensitivity made the isosbestic wavelength determination less accurate, and therefore it was not utilized in our spectral analysis. However, as shown later, the Cl_2O_2 cross section determined in this work is consistent with an isosbestic point near 271 nm.

On the basis of the observed isosbestic behavior the Cl_2O_2 absorption cross sections at 312.9 and 408.5 nm were determined using eq IV to be (3.69 ± 0.24) × 10^{-19} cm^2 $molecule^{-1}$ and (9.84 ± 1.85) × 10^{-21} cm^2 $molecule^{-1}$, respectively. The Cl_2O absorption cross sections at 200 K used in the isosbestic point analysis were σ_{Cl_2O}(312.9 nm) = 2.88 × 10^{-18} cm^2 $molecule^{-1}$ and σ_{Cl_2O}(408.5 nm) = 1.11 × 10^{-20} cm^2 $molecule^{-1}$.[12] The quoted uncertainty is at the 2σ (95% confidence) level and includes estimated systematic uncertainties in the Cl_2O and Cl_2 cross sections at these wavelengths and temperatures. Combining the Cl_2O_2 absorption cross section determined at the isosbestic points with the wavelength dependence of the Cl_2O_2 spectrum enables the determination of the peak absorption cross section as well as the absorption cross sections at other wavelengths (see section 3.3).

3.2. CT-TD Results. CT-TD experiments were performed with collection trap temperatures, T_C, of 138, 146, 148, 151, 153, and 155 K. The experimental conditions including [Cl_2] (~0.22 Torr), [O_3], photolysis photon flux, total flow rate, flow velocity, and collection time were similar in each experiment and only the collection trap temperature was changed. For the

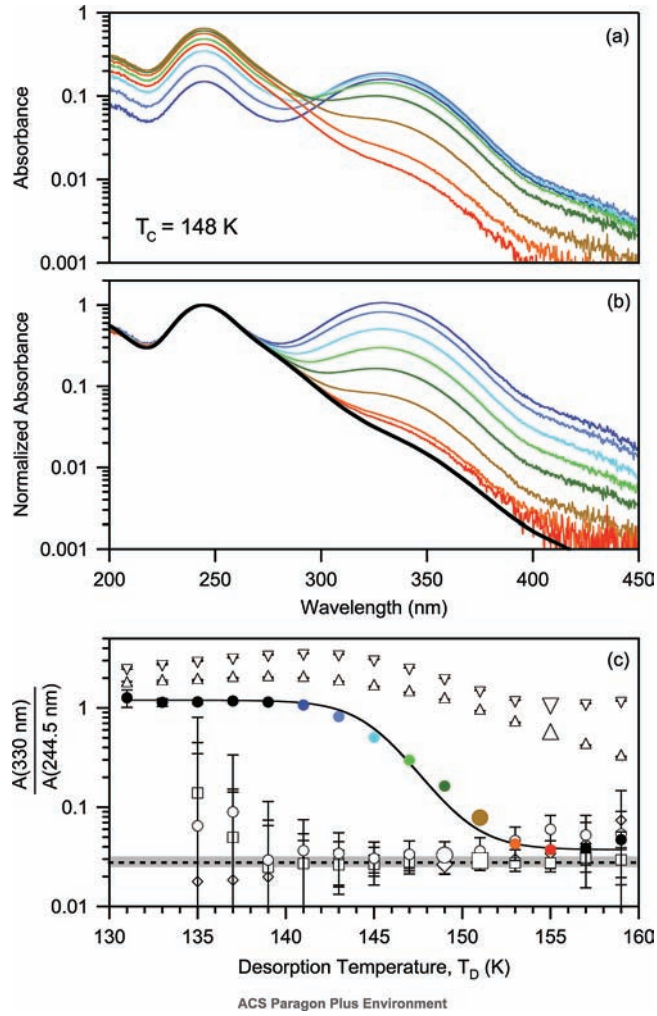

Figure 5. Results obtained in the cold trap thermal desorption (CT-TD) experiments. Frame a: Sequence of absorption spectra measured during thermal desorption of a sample collected at a trap temperature, T_C, of 148 K. The spectra color code is given in frame c. Frame b: The UV absorption spectra shown in frame a normalized at the peak of the Cl_2O_2 spectrum, 244.5 nm, showing the change in the Cl_2O_2/Cl_2 fractionation of the sample as the trap temperature increased. The heavy black curve is the Cl_2O_2 spectrum obtained in this work. Frame c: The ratio, A(330 nm)/A(244.5 nm), as a function of the desorption temperature, T_D, for samples collected at 138 K (▽), 146 K (△), 148 K (● and solid line) color coded to spectra shown in frames a and b, 151 K (□), 153 K (◇), and 155 K(○). The error limits shown are 2σ (95% confidence level) values from the absorption measurements. The larger size symbols indicate the desorption temperature where the maximum Cl_2O_2 absorption signal was observed. The dashed line and shaded 2σ uncertainty range is the ratio from the Cl_2O_2 spectrum obtained in the PLP-DA experiments in this work.

concentrations used, Cl_2 condensation was shown to be near our detection limit, for T_C >148 K. The absorption spectra and composition of the gas-phase sample as a function of T_C and desorption temperature, T_D, are summarized in Figure 5. Similar results were obtained using the 351 nm excimer laser as the photolysis light source although the production of Cl_2O_2 was significantly less. We have used the ratio of absorbances at 330 and 244.5 nm, A(330 nm)/A(244.5 nm), to evaluate the fractionation of the sample as a function of collection and desorption temperature. Smaller values of the ratio correspond to higher fractionation and purer gas-phase samples of Cl_2O_2. In the limit of a pure Cl_2O_2 sample, the ratio corresponds to the ratio of Cl_2O_2 absorption cross sections at these wavelengths. As shown in Figure 5 for T_C = 148 K, the ratio is nearly constant

for T_D <140 K but decreases rapidly at higher T_D and approaches an asymptotic value of 0.037. The ratio also shows a systematic decrease with increasing T_C. Measurements made with T_C >151 K yielded a ratio of 0.027 for all values of T_D; that is, the sample composition did not change with increasing T_D. The absolute Cl_2O_2 absorption signal increased with increasing T_D and reached maximum values for desorption temperatures in the range 148−155 K, depending slightly on T_C. For experiments with T_C <145 K the maximum Cl_2O_2 absorbance was the highest with values of ~1.4 at the peak (~2×10^{15} molecules cm^{-3}). At $T_D \approx 183$ K Cl_2O_2 and Cl_2 were completely removed from the trap and the measured spectrum returned to the initial background value (±0.001 absorbance unit). The approach to an asymptotic ratio with increasing T_D and T_C is consistent with a fractional distillation of the sample that reduces the amount of Cl_2 in the trapped sample at the higher T_C values. The absorption spectra measured throughout the desorption process were analyzed within the precision of the measurement to be due to contributions from only two absorbing species, Cl_2 and Cl_2O_2, for all conditions and temperatures shown in Figure 5. The lowest values of the ratio obtained using the CT-TD method, 0.027, correspond to an absorption spectrum that is in excellent agreement with the Cl_2O_2 spectrum obtained in our PLP-DA experiments, as shown in Figure 5.

The temperature dependence of the Cl_2O_2 spectrum was investigated over the range 201−218 K using Cl_2O_2 samples prepared using the CT-TD method with T_C = 151 K. A high trap collection temperature was used to minimize the Cl_2 contribution to the absorption spectrum. The Cl_2O_2 spectrum showed only small, <2%, changes over this very narrow temperature range. The weak temperature dependence of the Cl_2O_2 spectrum, particularly between 200 and 300 nm, implies that direct comparisons of the Cl_2O_2 spectra measured in this work with those reported in other studies but at slightly different temperatures can be made quantitatively.

Finally, a weak Cl_2O_3 absorption signal ($A < 0.01$ at 265 nm) was observed when T_D approached 200 K; Cl_2O_3 is less volatile than Cl_2O_2. In addition, near $T_D \approx 215$ K an unidentified low volatility condensate desorbed from the trap and condensed in the absorption cell. Absorption spectra recorded while using higher absorption cell temperatures eliminated the condensation, but we were unable to characterize the gas-phase absorption spectrum of the compound due to the very weak absorption signal. The formation of Cl_2O_3 or species other than Cl_2 and Cl_2O_2 when using the CT-TD method was not reported in previous studies using this method.[10,14] Test measurements performed using broad band photolysis, 320−800 nm, of the Cl_2/O_3 mixture led to significant production of OClO and Cl_2O_3. The amount of OClO and Cl_2O_3 produced was sensitive to the initial O_3 concentration in the reactor. It is most likely that photolysis of O_3 in the Chappuis band (400−700 nm) leads to the formation of O atoms and secondary chemistry leading to OClO and Cl_2O_3, although, additional studies are needed to identify the reaction mechanism. Optically filtering the photolysis wavelengths to 320−430 nm and minimizing the initial O_3 concentration reduced the production of OClO below our detection limit in most experiments.

3.3. Cl_2O_2 UV Absorption Spectrum Analysis. The Cl_2O_2 spectrum was determined using knowledge of the gas-phase chemistry and reaction stoichiometry combined with the isosbestic wavelengths observed in the PLP-DA experiments. The wavelength dependence of the Cl_2O_2 spectrum in the 200−280 nm region, where the contribution from Cl_2 absorption is negligible, was obtained using results from the PLP-DA experiments and sources 1−3 and the CT-TD experiments using source 3. The Cl_2O_2 spectrum in this wavelength region was also determined via the PLP-DA method using the previously reported location of the Cl_2O_2 absorption peak at 244.5 nm. The pulsed laser photolysis of Cl_2/O_3 mixtures at 351 nm, source 3, yielded low Cl_2O_2 concentrations, but reliable measurements of the Cl_2O_2 spectrum in the 200−280 nm range were obtained. Both experimental methods and the three Cl_2O_2 sources used yielded Cl_2O_2 spectra that were in excellent agreement, within 2%, in this wavelength region.

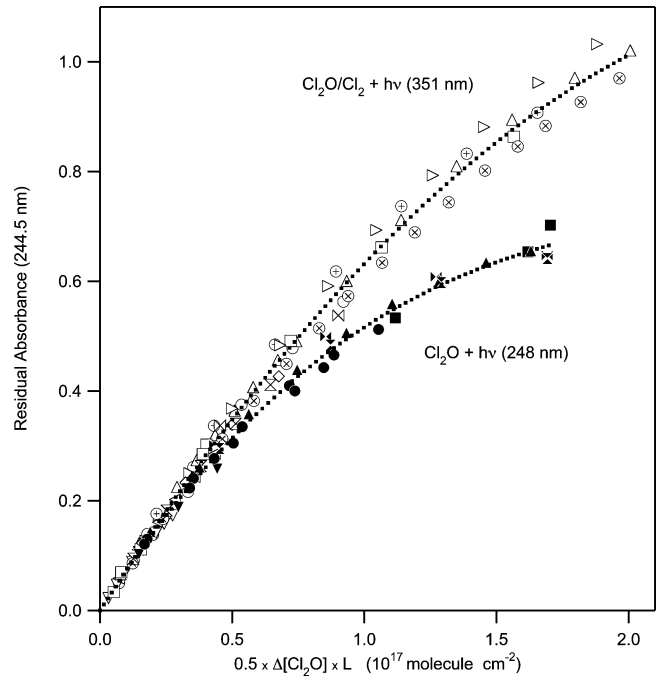

Figure 6. Data used in the determination of the Cl_2O_2 absorption cross section at 244.5 nm from the pulsed laser photolysis diode array absorption (PLP-DA) experiments using the 351 nm photolysis of Cl_2O/Cl_2 mixtures (open symbols) and the 248 nm photolysis of Cl_2O (solid symbols). The symbols represent individual experiments that were performed over a range of experimental conditions. The lines were obtained from a global least-squares fit to all the data. The initial slope yields a Cl_2O_2 absorption cross section, $\sigma_{Cl_2O_2} = \Delta A/(0.5\Delta[Cl_2O]L)$, at 244.5 nm of $(7.58 \pm 0.3) \times 10^{-18}$ cm^2 $molecule^{-1}$ where the quoted uncertainty is the 2σ precision of the fit.

The spectral subtraction of Cl_2O in each photolysis step of the PLP-DA experiments yields the change in Cl_2O concentration. The loss of Cl_2O is related to the formation of Cl_2O_2 and Cl_2 via the reaction stoichiometry (eqs II and III) described earlier

$$0.5\Delta[Cl_2O] = \Delta[Cl_2O_2] \qquad (V)$$

from which the cross sections for Cl_2O_2 in the wavelength range 200−280 nm were determined. Figure 6 shows a summary of the results obtained in the PLP-DA experiments for both sources 1 and 2. The experimental data follow the linear relationship of eq V at low Cl_2O conversion and negative curvature at higher Cl_2O conversion due to the loss of Cl_2O_2 (lower residual absorption), which is greater in the 248 nm photolysis experiments. Several experiments shown in Figure 6 were performed using multiple laser pulses per step and are indistinguishable from the results obtained using less photolysis per step. The initial slope, i.e., at low Cl_2O conversion, obtained from a least-squares polynomial fit to the data yielded a Cl_2O_2 absorption

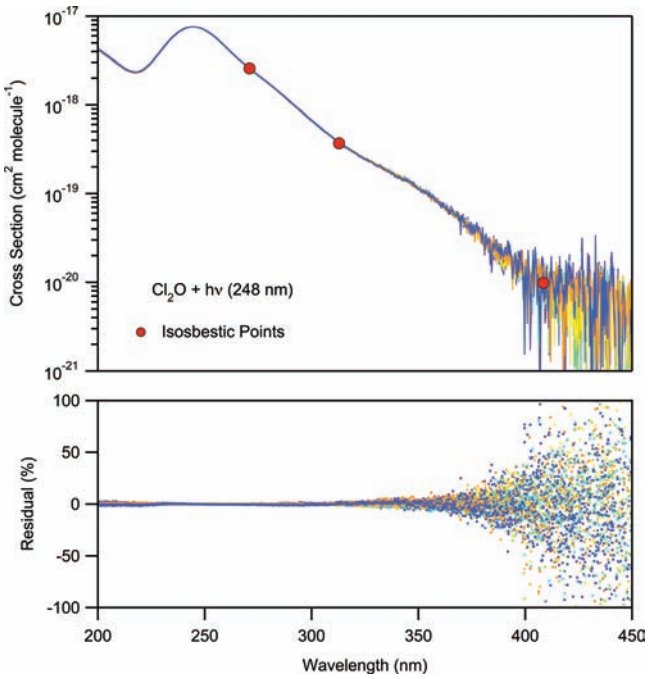

Figure 7. Cl_2O_2 UV absorption spectra obtained from the analysis of UV absorption spectra measured following the 248 nm pulsed laser photolysis of Cl_2O at 201 K and 725 Torr (He) (see text for details). The data points at 271, 312.9, and 408.5 nm (●) are the Cl_2O_2 absorption cross section values determined at the observed isosbestic points (see text). The lower frame shows the residuals of the spectra from the average. The residuals show deviations that are less than 2% between 200 and 300 nm, 5% between 300 and 350 nm, and increase toward longer wavelengths.

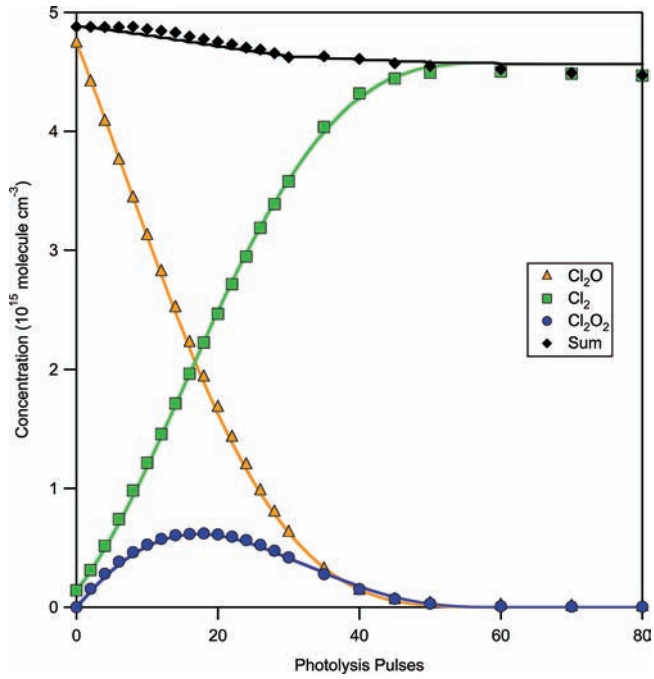

Figure 8. Temporal profiles of Cl_2O_2 (●), Cl_2O (▲), Cl_2 (■), and the sum (◆) obtained in a pulsed laser photolysis diode array absorption experiment at 201 K and 725 Torr (He). The lines shown were obtained from a simulation of the reaction system (see text for details).

cross section at 244.5 nm of (7.58 ± 0.3) × 10^{-18} cm^2 molecule^{-1} where the quoted error is the 2σ uncertainty of the fit. The absorption cross sections at other wavelengths between 200 and 280 nm were obtained relative to the peak value using the wavelength dependence of the Cl_2O_2 spectrum obtained in the PLP-DA and CT-TD experiments. The temporal profiles for Cl_2O_2, Cl_2O, and Cl_2 and the observed reaction mass balance are described later.

A similar absolute cross section determination method to that shown in Figure 6, eq V, was used to obtain a peak cross section for Cl_2, which is well-known. The peak Cl_2 absorption cross section obtained using PLP-DA data, source 1, agrees with the currently recommended value of 2.68 × 10^{-19} cm^2 molecule^{-1} [6] at 200 K with a standard deviation in seven determinations of 7%. The good agreement achieved for the peak cross section of Cl_2 confirms the self-consistency of the reaction stoichiometry used in the spectral analysis and that the Cl_2 absorption in our measured absorption spectra was accounted for accurately.

The determination of the Cl_2O_2 absorption spectrum at wavelengths >280 nm required the quantitative subtraction of absorption due to Cl_2. The Cl_2O_2 absorption spectrum at wavelengths >280 nm was determined using the cross sections at the isosbestic wavelengths combined with the cross section values obtained in the 200−280 nm region. Residual spectra were obtained for each photolysis step by subtracting Cl_2O and Cl_2 from the measured absorption spectrum. A typical set of residual spectra, normalized at 244.5 nm, the peak of the Cl_2O_2 spectrum, is shown in Figure 7. The agreement for the wavelength dependence of the residual absorption spectra, Cl_2O_2, at each photolysis step is excellent. The percent deviation of the residual spectra from the average, Figure 7, is less than 2% between 200 and 300 nm, 5% between 300 and 350 nm, and increases at longer wavelengths. The consistency of the absorption spectra for each photolysis step shows that the spectra measured in each photolysis step can be interpreted, within the precision of the measurements, by absorption from Cl_2O and Cl_2 and another species that we assign to Cl_2O_2. The residual spectra in Figure 7 show a precision that is typical for the various Cl_2O_2 sources and experimental conditions used in this study. The residual spectra obtained in the PLP-DA experiments and the spectrum obtained from method 2, for spectra with the ratio A(330 nm)/A(244.5 nm) = 0.027, are also in excellent agreement as shown in Figure 5.

The formation and stability of absorbing species other than Cl_2O_2, such as isomers of Cl_2O_2 (chloryl chloride, ClClOO) or Cl_2O_3, were evaluated by allowing a Cl_2O_2/Cl_2O/Cl_2 mixture to stand unperturbed in the absorption cell at 200 K for up to 20 min. The Cl_2O_2 concentration showed a first-order loss with a rate coefficient of ∼5 × 10^{-4} s^{-1}, but the wavelength dependence of the residual absorption spectrum remained constant. We conclude from these measurements that other chlorine species did not make a significant contribution to the measured absorption spectrum in this study.

3.3.1. Mass Balance. The partitioning and total chlorine mass balance (total = Cl_2O_2 + Cl_2O + Cl_2) for the PLP-DA spectra shown in Figure 3 is given in Figure 8. This data set is representative of the profiles obtained using sources 1 and 2. A simulation of the reaction system that included reactions 1–3, 5−11, and pseudo-first-order rate coefficients for the loss of Cl_2O_2 (5 × 10^{-4} s^{-1}) and Cl_2O (7 × 10^{-5} s^{-1}), as measured in this work, is included in Figure 8. The experimentally determined Cl_2O_2, Cl_2O, and Cl_2 temporal profiles are consistent with the behavior predicted by the reaction mechanism. Good agreement between the experimental data and simulated temporal profiles was obtained by allowing the photolysis laser fluence to vary ±5% from the measured value. It is worth noting that the concentrations of OClO and Cl_2O_3 calculated in the simulation are <1 × 10^{12} molecules cm^{-3} and therefore make negligible contributions to the measured UV absorption spectra.

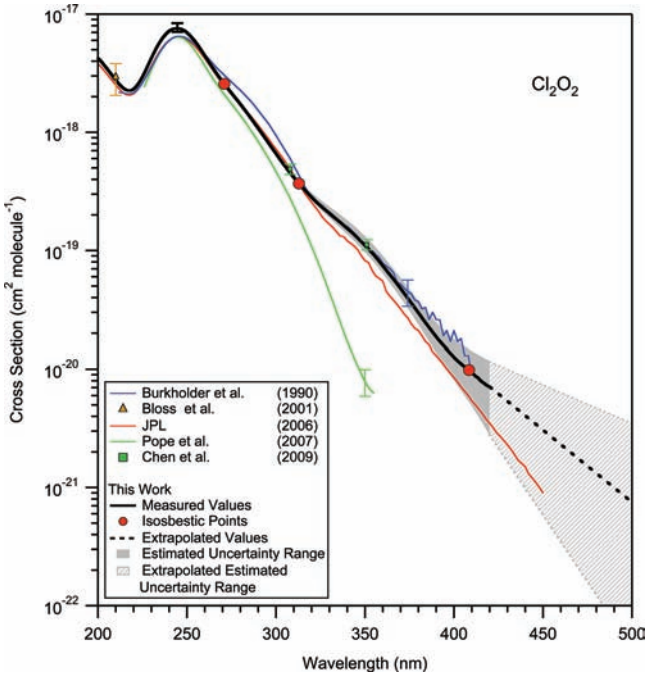

Figure 9. The Cl_2O_2 absorption spectrum obtained in this work (heavy black line) including the estimated error limits as a function of wavelength given by the shaded region (see text of discussion of error analysis). The absorption cross sections at the isosbestic points (271, 312.9, and 408.5 nm) from this work are also shown (red circles). The heavy dashed line gives an exponential extrapolation of our Cl_2O_2 cross section data beyond the range of our measurements. The light gray shaded region shows the extrapolation of the estimated cross section uncertainty. See the Supporting Information for the cross section data and extrapolation parameters. The absorption cross section data from Burkholder et al.[9] (blue line), Bloss et al.[17] (triangle), and Pope et al.[10] (green line) as well as the NASA/JPL recommendation[6] (red line) are included for comparison. The data from Chen et al.[19] (squares) at 308 and 351 nm are given assuming a Cl_2O_2 photolysis quantum yield of unity at these wavelengths.

The chlorine mass balance is very good, constant to within 1%, in the early stages of the experiment. However, following the maximum in Cl_2O_2 concentration a small systematic loss of total chlorine was observed in nearly all experiments with the loss at the end of the experiment being ~8%. The loss of total chlorine is reproduced reasonably well in the simulation when Cl_2O_2 and/or Cl_2O losses, either homogeneous or heterogeneous, that do not lead to the formation of gas-phase Cl_2 are included.

Several experiments were performed to examine the chlorine gas-phase loss in more detail. At the completion of a PLP-DA experiment the reaction cell was pumped out, sealed off, and warmed to room temperature. Cl_2 and a small amount of OClO were observed to gradually build up as the cell warmed. The total amount of Cl_2 accounted for the majority of the observed decrease in chlorine mass balance. We conclude that thermally unstable nonvolatile chlorine containing species were produced, either homogeneously or heterogeneously, in the later stages of the PLP-DA experiments. However, the UV absorption spectra measured in the later stages of an experiment yielded Cl_2O_2 absorption spectra that were identical to spectra recorded in the early stages. Therefore, the formation of unidentified compounds did not significantly influence the measured UV absorption spectra or the determination of the Cl_2O_2 absolute absorption cross sections in our experiments.

3.3.2. Cl_2O_2 Spectrum. The Cl_2O_2 absorption spectrum obtained in this study over the wavelength range 200−420 nm is shown in Figure 9 and listed in 0.5 nm intervals in the Supporting Information. The various experimental methods and chemical sources used in this study yielded Cl_2O_2 absorption spectra that were in very good agreement. The Cl_2O_2 absorption spectrum reported here was obtained from measurements near 200 K. The temperature dependence of the Cl_2O_2 absorption spectrum over the range 200−218 K was found to be small. The Cl_2O_2 UV absorption spectrum in the wavelength range 200−420 nm consists of several overlapping electronic bands. The spectrum peaks at 244.5 nm with a cross section value of 7.6×10^{-18} cm^2 $molecule^{-1}$. Toward shorter wavelengths the spectrum shows a minimum at ~218 nm and the onset of another strong absorption feature whose maximum is outside the wavelength range of our measurements. The absorption features at longer wavelength appear as shoulders on the main absorption band at 270 and 340 nm. The diffuse absorption band near 340 nm correlates with the Cl_2 absorption spectrum. Therefore, the accuracy of the Cl_2O_2 absorption spectrum in this wavelength region is dependent on accurately accounting for absorption by Cl_2. Although the uncertainty in our measurements at wavelengths longer than 380 nm is large, >50%, the observation of an isosbestic point at 408.5 nm in our experiments indicates that Cl_2O_2 absorbs in this wavelength region.

3.4. Error Analysis. Systematic and absolute uncertainties in our measurements affect both the wavelength dependence of the Cl_2O_2 absorption spectrum and its absolute absorption cross sections. The high precision of our absorption measurements was the result of the stability of the D_2 lamp intensity and optical setup. In the wavelength range 200−280 nm, the uncertainty in the Cl_2O_2 absorbance due to the measurement precision was small, <1%. At longer wavelengths where the absorption cross sections for Cl_2O_2 are smaller, the measurement precision makes a larger contribution to the overall uncertainty: ~2% at 300 nm, ~5% at 350 nm, and ~50% for λ >400 nm. Figure 9 shows the Cl_2O_2 absorption spectrum obtained in this work along with the estimated uncertainty as a function of wavelength. The estimated uncertainty in the Cl_2O_2 absolute cross sections is 5−10% (2σ confidence level) at and around the peak of the Cl_2O_2 spectrum, near 245 nm. A parametrization for the estimated uncertainties in the actinic region is given in the Supporting Information. The estimated uncertainty includes the uncertainty associated with the spectral subtraction of Cl_2O and Cl_2, which does not contribute significantly to the overall uncertainty, <1%. The uncertainty in the isosbestic wavelength at 312.9 nm is estimated to be +0.3/−0.5 nm. The Cl_2O_2 spectrum obtained using the lower limit of the isosbestic wavelength in the spectral analysis would increase the Cl_2O_2 cross section in the wavelength region 330−350 nm as a result of smaller Cl_2 subtraction. The increase would be 16% at 350 nm for an isosbestic wavelength of 312.4 nm and a decrease of 10% for an isosbestic wavelength of 313.2 nm.

The presence of unaccounted for impurities was examined experimentally and determined to be negligible. The most likely impurities are OClO and Cl_2O_3 while ClClOO and other chlorine oxides were also considered. OClO, which has a strong and readily detectable structured UV/vis absorption band, did not make a significant contribution to our measured spectra. We estimate that Cl_2O_3 made a negligible contribution, <1% at 265 nm, to our measured absorption spectra. ClClOO, an isomer of Cl_2O_2, absorbs strongly in the UV. On the basis of our detection limit for ClClOO, $\sim 7 \times 10^{11}$ molecules cm^{-3}, we estimate that its contribution to the measured absorption spectra was <1% at all wavelengths.

The influence of secondary chemistry is difficult to quantitatively evaluate. The high degree of consistency for the residual

TABLE 1: Summary of Cl_2O_2 UV Absorption Spectrum Studies

reference	year	temperature (K)	technique	wavelength (λ) (nm)	$10^{20}\sigma(\lambda)$ (cm^2)
Cox and Hayman[15]	1988	200−300	BB-DA	220−360	640 ± 60^a
Burkholder et al.[9]	1990	205−250	DF-DA/FTIR	212−410	650^{+80a}_{-50}
DeMore and Tschuikow-Roux[13]	1990	206	BB-DA	190−400	680 ± 80^a
Huder and DeMore[16]	1995	195	BB-DA	200−310	$-^{b,d}$
Bloss et al.[17]	2001	183−245	PLP-TA	210	294 ± 86
Pope et al.[10]	2007	193	CT-TD	226−355	$-^b$
von Hobe et al.[14]	2009	10	MI	220−400	$-^{b,c}$
Chen et al.[19]	2009	200	PLP-MS	308	49^e
		250		308	50.9
		200		351	11.2
		250		351	12.6
this work	2009	200−228	PLP-DA CT-TD	200−450	760^{+80a}_{-50}

[a] Absorption cross section value at the peak of the spectrum, $\lambda = 245$ nm. Cross section data reported over the range of wavelengths given. [b] Reported Cl_2O_2 absorption spectrum normalized to the recommended peak absorption cross section. [c] Cl_2O_2 absorption spectrum measured in a Ne matrix. [d] Cl_2O_2 absorption spectrum reported at $\lambda > 310$ nm is reported in Huder and DeMore using a log−linear extrapolation of values measured at shorter wavelengths. [e] Cl_2O_2 cross section calculated here assuming a unit Cl_2O_2 photolysis quantum yield at these wavelengths. BB, broad band photolysis; DA, diode array spectroscopy; DF, discharge flow; FTIR, Fourier transform infrared spectroscopy; PLP, pulsed laser photolysis; TA, transient absorption; MS, mass spectrometry, CT-TD, cold trap thermal desorption; MI, matrix isolation.

absorption spectra obtained in the PLP-DA experiments suggests however that it is small. The photolysis of Cl_2O at 248 nm is reported to yield >90% Cl atoms. Therefore, a small yield of O atoms is possible. O atoms would react with the Cl_2O that is present in large excess initially

$$O + Cl_2O \rightarrow ClO + ClO \quad (13)$$

where $k_{13}(T) = 2.7 \times 10^{-11} \exp(-530/T)$ cm^3 $molecule^{-1}$ s^{-1}, $k_{13}(200\ K) = 1.6 \times 10^{-12}$ cm^3 $molecule^{-1}$ s^{-1}. The formation of two ClO radicals and loss of Cl_2O lead to the same overall reaction stoichiometry as obtained if no O atoms were formed. In subsequent photolysis steps O atoms could possibly react with Cl_2O_2

$$O + Cl_2O_2 \rightarrow \text{products} \quad (14)$$

where the rate coefficient for this reaction is currently unknown. The agreement between our results obtained using Cl_2O (248 nm) and Cl_2/Cl_2O (351 nm) photolysis sources indicates the possible small yield of O atoms in reaction 6 did not influence the determination of the Cl_2O_2 spectrum significantly.

In addition to the uncertainties associated with the absorption measurements and spectral analysis, the breakdown of the reaction stoichiometry due to loss of ClO or Cl_2O_2 influences our results. It is difficult to estimate this uncertainty, but it is probably <10%. The stoichiometry was shown to be valid for Cl_2 where we obtained good agreement for its peak cross section with the recommended value. Unaccounted for loss of Cl_2O_2 or ClO would lead to an overestimation of the Cl_2O_2 concentration and consequently an underestimation of the peak Cl_2O_2 absorption cross section. Finally, the Cl_2O_2 absorption cross section at the peak of the spectrum is $7.6^{+0.8}_{-0.5} \times 10^{-18}$ cm^2 $molecule^{-1}$ were the quoted uncertainties are at the 2σ level and include estimated systematic errors.

3.5. Comparison with Previous Studies. There are a number of published studies of the Cl_2O_2 UV absorption spectrum,[9,10,13−16] its absolute cross section values,[9,13,15,17] and photolysis products and quantum yields[7,8,18,19] that we can compare with the present work. A summary of previously reported Cl_2O_2 UV absorption spectrum data is given in Figure 1 and summarized in Table 1. The spectrum recommended by NASA/JPL[6] for use in atmospheric modeling studies is included in Figures 1 and 9 for comparison purposes. The IUPAC[20] evaluation panel currently recommends the Cl_2O_2 spectrum and extrapolation for the long wavelength region reported in Huder and DeMore.[16] The discrepancies among the previous studies and comparison with the results from the present study are discussed here.

Although there have been numerous studies of the Cl_2O_2 UV absorption spectrum reported over the past 30 years, the overall level of agreement among the various data sets is rather poor. The scatter in the data is primarily associated with difficulties in preparing, purifying, and handling gas-phase samples of the transient Cl_2O_2 molecule and measuring its weak absorption cross sections in the actinic region. The scatter in the laboratory data translates directly into uncertainties in the calculated atmospheric photolysis rate for Cl_2O_2. The highest level of agreement among these studies is in and around the peak of the Cl_2O_2 spectrum near 245 nm, with differences of <10% in most cases. Note that several of the studies shown in Figure 1 do not include absolute cross section determinations and have been normalized to the peak cross section recommended by NASA/JPL. As shown in Figure 1, the largest discrepancies are in the long wavelength region, $\lambda > 300$ nm, which is the region most important for calculating atmospheric photolysis rates.

The studies of Cox and Hayman,[15] Burkholder et al.,[9] and DeMore and Tschuikow-Roux[13] report high Cl_2O_2 cross section values in the 250−300 nm range and may have been influenced by spectral impurities, the primary impurity being Cl_2O, which was used as a radical precursor, while the Cox and Hayman[15] and Burkholder et al.[9] studies also show evidence for the possible interference from Cl_2O_3. For $\lambda > 300$ nm, Pope et al.[10] reported the lowest Cl_2O_2 cross section values, while Burkholder et al.[9] has reported the highest values. The differences are large, nearly a factor of 10 at 350 nm, which results in substantial and significant differences in the calculated atmospheric photolysis rates. It is worth noting that the studies prior to Pope et al.[10] also show discrepancies in this wavelength region, Figure 1, although the differences are much smaller. The Cl_2O_2 spectrum obtained in the present work is in excellent agreement with results from Burkholder et al. for $\lambda > 300$ nm. Chen et al.[19] used a newly developed experimental technique that combined pulsed laser photolysis in a molecular beam with mass spectrometric detection of Cl_2O_2. Their experiments measured the

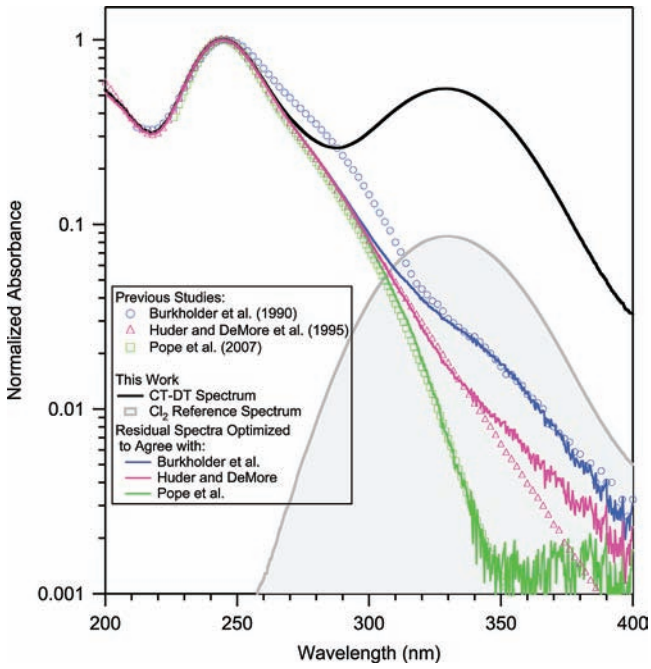

Figure 10. Illustration of the sensitivity of the Cl_2O_2 spectral analysis to the Cl_2 spectral subtraction and the level of agreement that can be obtained with representative Cl_2O_2 spectra reported in the literature. The experimental spectrum was recorded using the CT-TD method and contains a large contribution from Cl_2 as seen by the peak in the spectrum at 330 nm. An optimized agreement of residual spectra (lines) obtained by subtracting Cl_2 absorption from the experimental spectrum with the Cl_2O_2 spectra reported by Burkholder et al. (○),[9] Huder and DeMore (△),[16] and Pope et al. (□)[10] are shown.

product of the Cl_2O_2 absorption cross section and its photolysis quantum yield, $\sigma_{Cl_2O_2}(\lambda)\Phi(\lambda)$. The experimental method is independent of Cl_2 and therefore not susceptible to uncertainties associated with possible Cl_2 impurities as discussed below. Values of $\sigma_{Cl_2O_2}(\lambda)\Phi(\lambda)$ reported for wavelengths of 308 and 351 nm are in excellent agreement with the present Cl_2O_2 cross section values, within 7%, when $\Phi(\lambda)$ is assumed to be unity. The good agreement between the Chen et al.[19] results and those obtained here provide additional evidence that the methods used in the present work to account for Cl_2 are valid.

3.5.1. Cl_2 Spectral Interference. A source of uncertainty in the reported Cl_2O_2 spectra is associated with the uncertainties in corrections for Cl_2 absorption. Cl_2 is present as an impurity in all gas-phase Cl_2O_2 spectrum studies reported to date, and measured spectra must account for its contribution to obtain accurate cross section values at λ >300 nm. The point that differences in Cl_2 subtraction alone can account for the majority of the discrepancies in the Cl_2O_2 cross section at λ >300 nm is illustrated in Figure 10 using experimental data obtained in this study. In this example, an absorption spectrum containing significant Cl_2 absorption was taken from our CT-TD experiments. We compared the residual normalized spectra obtained following Cl_2 subtraction with the highest (Burkholder et al.[9]), intermediate (Huder and DeMore[16]), and lowest (Pope et al.[10]) Cl_2O_2 spectra reported in the wavelength range >300 nm. Subtracting various amounts of Cl_2 on a subjective basis, using a Cl_2 reference spectrum recorded under identical conditions, we obtain the Cl_2O_2 spectrum obtained in this work and good agreement with the Cl_2O_2 spectrum reported by Burkholder et al.[9] Increasing the amount of Cl_2 subtraction yields reasonable agreement with the exponential extrapolation given by Huder and DeMore[16] although systematic deviations are observed. Increasing the amount of Cl_2 subtraction further yields reasonable agreement with the Cl_2O_2 spectrum reported by Pope et al.,[10] although the residual spectrum contains slightly negative values at the longer wavelengths. The difference in the amount of Cl_2 subtraction needed to obtain the residuals that agree with the Burkholder et al.[9] and Pope et al.[10] spectra was only 4.5%. This exercise highlights the need for accurate methods to account for Cl_2 in the determination of the Cl_2O_2 spectrum.

Prior to the Pope et al.[10] study, only Burkholder et al.[9] and DeMore and Tschiukow-Roux[13] had reported absorption cross section data for wavelengths >320 nm. As shown in Figure 10, the uncertainty in the magnitude of the Cl_2 corrections can account for the majority of the discrepancies in the reported Cl_2O_2 spectra. Burkholder et al.[9] used a discharge flow chemical titration method to determine the Cl_2 contribution to their measured absorption spectra. They estimated the uncertainty in their Cl_2O_2 absorption cross section at 330 nm to be in the range 10−15%. DeMore and Tschiukow-Roux[13] corrected their measured spectra for Cl_2 absorption using a subjective iterative spectral subtraction approach. They report the uncertainty in their Cl_2O_2 cross section to be ∼30% at ∼350 nm. Pope et al.[10] fit their measured absorption spectra, which contained both Cl_2O_2 and Cl_2, using two Gaussian profiles and a reference Cl_2 absorption spectrum. The fitting procedure optimized the parameters of the Gaussian functions (peak location and width, in wavelength space) and the abundance of Cl_2. On the basis of their measurement precision, they estimated the uncertainty in the Cl_2O_2 cross section at ∼350 nm to be ∼25%. The absolute uncertainties in their Cl_2O_2 absorption cross sections in the long wavelength region are most likely larger and dependent on the validity of the assumptions applied in the spectral fitting, which are difficult to quantify. In such a spectral analysis approach, a correlation between the UV absorption spectra of Cl_2 and Cl_2O_2 would lead to systematic errors in the Cl_2O_2 spectrum obtained. In our work, we obtained UV absorption spectra using the CT-TD method that contained Cl_2 and Cl_2O_2 that are consistent with those reported by Pope et al.,[10] who used the same experimental method. Therefore, the source of the discrepancies in the reported Cl_2O_2 spectra between the two studies is not the result of the spectral measurements themselves but lies in the interpretation of the measured spectra, as illustrated in Figure 10. In our work, we have also shown that absorption spectra obtained using the CT-TD method at trapping temperatures greater than 151 K are consistent with our PLP-DA experiments, Figure 5. In conclusion, the major source of the discrepancy between our work and that of Pope et al.[10] is attributed to the uncertainty in the Cl_2 subtraction. In the present study our methods were designed to quantitatively account for Cl_2 interference by using the observed isosbestic wavelengths, reaction stoichiometry, and chlorine mass balance.

von Hobe et al.[14] reported a Cl_2O_2 absorption spectrum measured in a 10 K Ne matrix, shown in Figure 1. Cl_2O_2 samples were prepared using the CT method, and samples purified by vacuum distillation were shown to contain negligible amounts of Cl_2. The wavelength dependence of the spectrum at λ <300 nm is in good agreement with that from this work although the width of the absorption band is narrower due to the much lower temperature of the matrix measurement. In the long wavelength region, von Hobe et al. report Cl_2O_2 absorption at wavelengths out to 400 nm, which is consistent with our gas-phase observations that Cl_2O_2 absorbs in this wavelength region. Their Cl_2O_2 spectrum (normalized to a peak cross section of 6.5×10^{-18} cm^2 $molecule^{-1}$) is a factor of 2 lower than the value reported in this work and a factor of 7 greater than the value reported by Pope et al.[10] at 350 nm.

Absolute cross section values for Cl_2O_2 have been reported by Cox and Hayman,[15] Burkholder et al.,[9] DeMore and Tschiukow-Roux,[13] and Bloss et al.[17] The peak absorption cross section values in these studies are systematically lower than the value obtained in this work, $7.6^{+0.8}_{-0.5} \times 10^{-18}$ cm^2 molecule^{-1}, although all the reported values fall within the combined 2σ error limits. The cross sections reported by Bloss et al.[17] and Chen et al.[19] (assuming a unity quantum yield) are in excellent agreement, within 7%, with the values obtained in this work.

For the actinic region, the Cl_2O_2 absorption spectrum reported in this work is in good agreement with spectra reported by Burkholder et al.[9] and the values reported by Chen et al.[19] for 308 and 351 nm. These studies used different experimental techniques and obtained consistent Cl_2O_2 cross section data. Our spectrum is systematically larger than that reported by DeMore and Tschiukow-Roux[13] although the two data sets overlap within the combined uncertainties. This work and the studies of Burkholder et al.,[9] Chen et al.,[19] and DeMore and Tschiukow-Roux[13] report Cl_2O_2 absorption cross section values obtained using different experimental techniques that are significantly greater than those reported in the Pope et al.[10] study.

4. Atmospheric Implications

In the winter/spring Antarctic polar vortex, the ClO dimer catalytic ozone destruction cycle, reactions 1−4, accounts for the majority of calculated ozone depletion.[4] In the Arctic polar stratosphere, the photochemistry of Cl_2O_2 is also important although the extent of ozone depletion is less due to the meteorological variability in the winter vortex. A critical parameter in determining the efficiency of the ClO dimer cycle is the atmospheric photolysis rate coefficient, J, of Cl_2O_2 which is calculated from the product of the Cl_2O_2 absorption cross section, its photolysis quantum yield, and the solar flux integrated over all wavelengths

$$J = \int J(\lambda)\, d\lambda = \int \sigma(\lambda)\Phi(\lambda)\Psi(\lambda,Z,\chi)\, d\lambda \qquad \text{(VI)}$$

where $\sigma(\lambda)$ is the absorption cross section of Cl_2O_2 at wavelength λ, $\Phi(\lambda)$ is the photolysis quantum yield of Cl_2O_2, and $\Psi(\lambda,Z,\chi)$ is the solar flux which is a function of wavelength, altitude (Z), and solar zenith angle (SZA, χ). It is worth noting that the efficiency of the ClO dimer cycle also influences the efficiency of the ClO + BrO catalytic ozone destruction cycle

$$Cl + O_3 \rightarrow ClO + O_2 \qquad (4)$$

$$Br + O_3 \rightarrow BrO + O_2 \qquad (15)$$

$$ClO + BrO \rightarrow Cl + Br + O_2 \qquad (16)$$

$$\text{NET } 2O_3 \rightarrow 3O_2$$

by altering the atmospheric abundance of ClO.

$J(\lambda)$ values calculated for a SZA of 86° and altitude of 20 km, representative conditions for stratospheric measurements of ClO and Cl_2O_2 in the Arctic, with the Cl_2O_2 cross section data from this work and from several previous studies (Burkholder et al.,[9] NASA/JPL,[6] and Pope et al.[10]) is given in Figure 11. These studies were chosen because they represent the highest, currently recommended, and lowest Cl_2O_2 cross section data available for the long wavelength region. For the wavelength region longer than the experimentally available values an exponential extrapolation was used as shown in Figure 9. The wavelength-dependent solar fluxes were obtained using the NCAR online TUV calculator.[21] $J(\lambda)$ has a maximum between 330 and 340 nm and falls to nearly zero at 300 nm. The absolute magnitude of $J(\lambda)$ and the decrease toward longer wavelength differ for the different Cl_2O_2 cross section data sets as expected. The Pope et al.[10] cross section data set results in the lowest maximum value of $J(\lambda)$. The data sets from this work and Burkholder et al.[9] yield similar magnitude $J(\lambda)$ values while the NASA/JPL[6] values have a similar wavelength dependence but are systematically lower.

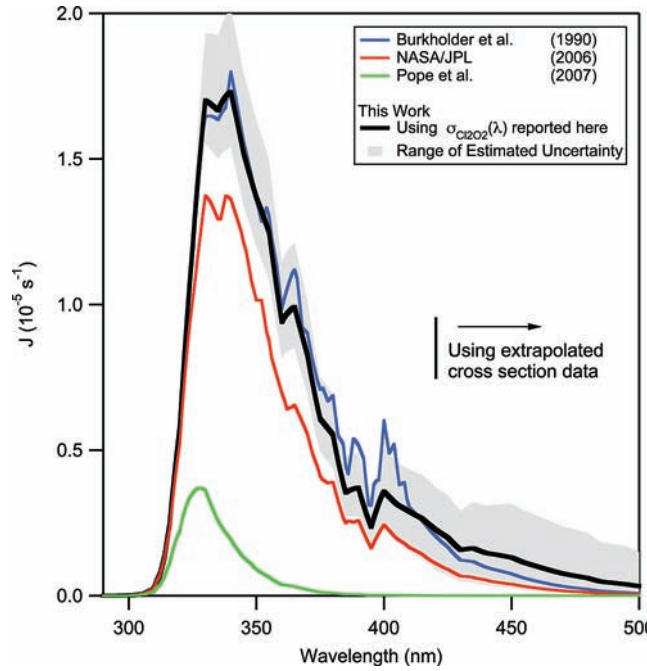

Figure 11. Comparison of wavelength-dependent Cl_2O_2 atmospheric photolysis rate coefficients, $J(\lambda)$, calculated for a solar zenith angle (SZA) of 86° at an altitude of 20 km using the Cl_2O_2 UV absorption cross obtained in this work (heavy black) where the upper and lower limits of the shaded region were calculated using the estimated uncertainty limits for the Cl_2O_2 cross section data reported in this study and shown in Figure 9 (see text for details of the error analysis). $J(\lambda)$ values calculated using previously reported Cl_2O_2 cross section data are included for comparison: Burkholder et al.[9] (blue), NASA/JPL[6] (red), and Pope et al.[10] (green). Solar fluxes were calculated using the online NCAR TUV calculator.[21]

$J(\lambda > 350$ nm) is significant for the Cl_2O_2 cross section data from this work, Burkholder et al.,[9] and NASA/JPL.[6] $J(\lambda > 420$ nm), i.e., beyond the limit of our experimental data, makes a non-negligible, ~10−30%, contribution to the total photolysis rate coefficient. The long wavelength contribution depends on the SZA and will also depend on the subjective method used to extrapolate the cross section data. Pope et al.[10] report Cl_2O_2 cross section data that decreases significantly at wavelengths greater than 300 nm with reported values extending out to 360 nm. Including an extrapolation of their cross section data to longer wavelengths increases the calculated total photolysis rate coefficient only slightly. The differences in the photolysis rate coefficients calculated for the cross section data from Pope et al.[10] and this work have significant implications for atmospheric model calculated ClO_x abundance and ozone loss rates.

The uncertainties in the Cl_2O_2 absorption cross sections from this work, as a function of wavelength, are shown in Figure 9. We extended the estimated uncertainty limits beyond 420 nm using an exponential extrapolation, shown in Figure 9, in order

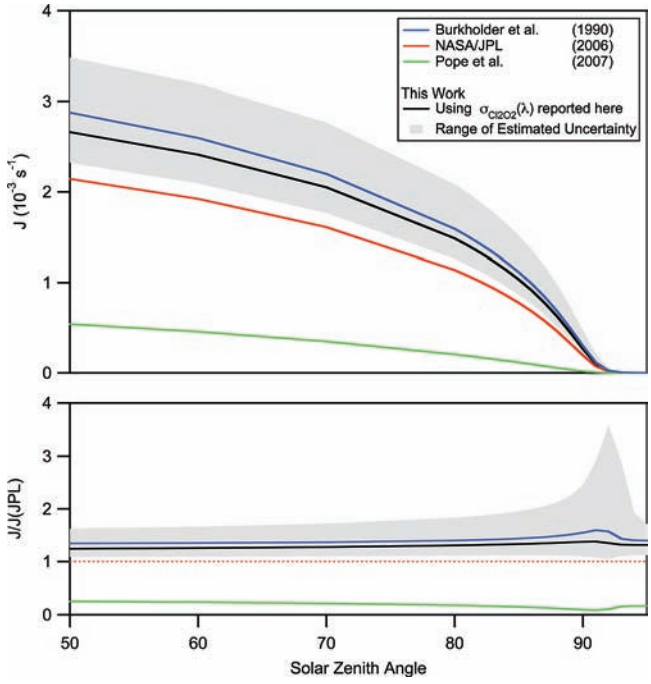

Figure 12. The upper frame shows the integrated atmospheric photolysis rate coefficients, J, calculated for Cl_2O_2 as a function of solar zenith angle (SZA) using the UV absorption cross section data from this work (black). The upper and lower limits of the shaded region were calculated using the estimated uncertainty limits for the Cl_2O_2 cross section data reported in this study and shown in Figure 9 (see text for details of the error analysis). J values calculated using the Cl_2O_2 cross section data from Burkholder et al.[9] (blue), NASA/JPL[6] (red), and Pope et al.[10] (green) are included for comparison. Solar fluxes were calculated using the online NCAR TUV calculator.[21] The lower frame shows the same data relative to the values obtained using the NASA/JPL recommended Cl_2O_2 cross section data.

to quantify the impact on the overall Cl_2O_2 atmospheric photolysis rate coefficient. The $J(\lambda)$ values obtained using the upper and lower limits of the cross section data in eq VI are shown in Figure 11. As expected, the uncertainty in $J(\lambda > 420$ nm) is large due to the large uncertainty in the Cl_2O_2 absorption cross section at these wavelengths. It is also worth noting that including the extrapolated Cl_2O_2 cross section data as shown in Figure 9 leads to asymmetric uncertainty limits in $J(\lambda)$. For a SZA of 86°, shown in Figure 11, $J(\lambda > 420$ nm) accounts for ~23% of the total photolysis rate coefficient. The range of uncertainty in $J(\lambda)$ using the Cl_2O_2 cross section data reported here is approximately +50%/−20% at the 2σ confidence level. The estimated uncertainty in $J(\lambda < 420$ nm) is ±18% at the 2σ confidence level. Thus, our estimated lower limit for the photolysis rate coefficient is only slightly dependent on the extrapolation of the Cl_2O_2 cross section data to wavelengths >420 nm. The estimated upper limit for J is, however, dependent on the extrapolated Cl_2O_2 cross section data. The extrapolation method used here most likely yields a maximum to the upper limit of the Cl_2O_2 cross section values for wavelengths >420 nm. Including the upper limit extrapolated Cl_2O_2 cross section data increases the overall photolysis rate by ~50%. Reduction of the uncertainty in the Cl_2O_2 atmospheric photolysis rate coefficient below the 50% level requires improved knowledge of the Cl_2O_2 absorption cross sections and photolysis quantum yields at wavelengths >420 nm.

Figure 12 shows the photolysis rate coefficients, J, integrated over the wavelength range 290−725 nm as a function of SZA for Cl_2O_2 cross section data from the present work, Burkholder et al.,[9] NASA/JPL,[6] and Pope et al.[10] The J values obtained using the present Cl_2O_2 spectrum and that of Burkholder et al.[9] agree very well, within ~10%, which is within the combined uncertainties of the Cl_2O_2 cross section values for the two studies. The J values from the present work are ~30% higher than NASA/JPL and a factor of 9 greater than those obtained using the Pope et al.[10] data for SZA < 80°. At larger SZAs the differences between this work and NASA/JPL[6] and Pope et al.[10] are greater. These differences have a significant impact on atmospheric model calculated ClO_x abundance and ozone loss rates as shown in previous atmospheric model studies of polar stratospheric halogen chemistry.[4,22,23] The uncertainty in the J(SZA) values, shown in Figure 12, increases with SZA from +50%/−20% at 86° to a maximum at ~92°.

The present Cl_2O_2 absorption cross section data are in close agreement with the data previously reported by Burkholder et al.[9] for $\lambda > 300$ nm. We point out the similarity with the previous Burkholder et al.[9] study primarily because previous modeling studies of polar stratospheric in situ and remote sensing measurements have frequently included the Burkholder et al.[9] Cl_2O_2 cross section data in their analysis. Therefore, we can draw meaningful conclusions here from the previous model studies by a direct comparison with the Burkholder et al.[9] cross section data. von Hobe et al.[23] recently provided a summary of ClO_x Arctic field measurements and an atmospheric model analysis using different photochemical input parameters including the Cl_2O_2 absorption cross section data from Burkholder et al.[9] The available ClO_x field measurement data sets, unfortunately, do not provide a consistent enough picture of ClO_x in the Arctic to make an evaluation of Cl_2O_2 cross section data from field measurements alone. However, von Hobe et al.[23] concluded that the "best" agreement between model and observations was obtained for Cl_2O_2 photolysis rates falling between the Burkholder et al.[9] and the NASA/JPL[6] recommendations, while using the Pope et al.[10] Cl_2O_2 cross section data resulted in very poor agreement. If the Pope et al.[10] cross section data are correct, it would therefore require including unknown chemical processes to explain the discrepancies between models and observations. In another study, Frieler et al.[4] calculated ozone loss in the Arctic and Antarctic vortices using various photochemical input parameters. They obtained good quantitative agreement with field observations when using Cl_2O_2 photolysis rates calculated using the Burkholder et al.[9] data combined with increased levels of Br_x loading, ~6 ppt.

5. Concluding Remarks

The UV absorption spectrum of Cl_2O_2 was measured in the present study over the wavelength range 200−420 nm at 200−228 K. The present study was designed to quantitatively account for Cl_2 spectral interference by using the observed isosbestic wavelengths, reaction stoichiometry, and chlorine mass balance. The Cl_2O_2 absorption cross section at the peak of the spectrum, 244.5 nm, was determined to be $7.6^{+0.8}_{-0.5} \times 10^{-18}$ cm^2 $molecule^{-1}$, which is ~17% larger than that currently recommended by NASA/JPL[6] and IUPAC.[20] The cross sections in the long wavelength region of the spectrum agree reasonably well with the values reported by Burkholder et al.[9] but are in poor agreement with those reported in the recent study by Pope et al.[10] The Cl_2O_2 absorption spectrum and cross section values obtained in this study yield atmospheric photolysis rate coefficients that are of similar magnitude to those calculated using the data from Burkholder et al.[9] The stratospheric photolysis rate coefficients obtained from this work are ~30% greater than those obtained using the NASA/JPL[6] recommended Cl_2O_2 cross section values. The present results provide strong evidence that

the recent study by Pope et al.[10] underestimated the Cl_2O_2 absorption in the wavelength region 300−400 nm, the region most important for atmospheric photolysis rate calculations. It has been suggested that if the Pope et al.[10] results were correct, then significant gaps in our current understanding of polar stratospheric chemistry and ozone depletion mechanisms exist. Although improvements in our fundamental understanding of the photochemistry of Cl_2O_2 are still desired, our work indicates that major revisions in current atmospheric chemical mechanisms are not required to simulate observed polar ozone depletion.

Acknowledgment. We thank SPARC for organizing the "The Role of Halogen Chemistry in Polar Stratospheric Ozone Depletion" workshop and supporting discussion on this topic. This work was supported in part by NOAA's Climate Goal and in part by NASA's Atmospheric Composition, Upper Atmospheric Research Program.

Supporting Information Available: Tabulated Cl_2O_2 absorption cross section data obtained in this work, parameterization of the wavelength-dependent estimated uncertainties in the Cl_2O_2 absorption cross section values, and simulations of isosbestic point behavior obtained using a chemical reaction mechanism. This material is available free of charge via the Internet at http://pubs.acs.org.

References and Notes

(1) Scientific Assessment of Ozone Depletion: 2006, Global Ozone Research and Monitoring Project; World Meteorological Organization: Geneva, URL http://www.wmo.int/pages/prog/arep/gaw/ozone_2006/ozone_asst_report.html.

(2) Solomon, S. *Rev. Geophys.* **1999**, *37*, 275.

(3) Newman, P. A.; Nash, E. R.; Kawa, S. R.; Montzka, S. A.; Schauffler, S. M. *Geophys. Res. Lett.* **2006**, *33*, L12814.

(4) Frieler, K.; Rex, M.; Salawitch, R. J.; Canty, T.; Streibel, M.; Stimpfle, R. M.; Pfeilsticker, K.; Dorf, M.; Weisenstein, D. K.; Godin-Beekmann, S. *Geophys. Res. Lett.* **2006**, *33*, L10812.

(5) Molina, L. T.; Molina, M. J. *J. Phys. Chem.* **1987**, *91*, 433.

(6) Sander, S. P.; Friedl, R. R.; Golden, D. M.; Kurylo, M. J.; Moortgat, G. K.; Keller-Rudek, H.; Wine, P. H.; Ravishankara, A. R.; Kolb, C. E.; Molina, M. J.; Finlayson-Pitts, B. J.; Huie, R. E.; Orkin, V. L. *Chemical kinetics and photochemical data for use in atmospheric studies*; JPL Pub. 06-2, Jet Propulsion Laboratory: Pasadena, CA, 2006; Vol. Evaluation Number 15.

(7) Molina, M. J.; Colussi, A. J.; Molina, L. T.; Schlindler, R. N.; Tso, T. L. *Chem. Phys. Lett.* **1990**, *173*, 310.

(8) Plenge, J.; Flesch, R.; Kühl, S.; Vogel, B.; Müller, R.; Stroh, F.; Rühl, E. *J. Phys. Chem. A* **2004**, *108*, 4859.

(9) Burkholder, J. B.; Orlando, J. J.; Howard, C. J. *J. Phys. Chem.* **1990**, *94*, 687.

(10) Pope, F. D.; Hansen, J. C.; Bayes, K. D.; Friedl, R. R.; Sander, S. P. *J. Phys. Chem. A* **2007**, *111*, 4322.

(11) *Stratospheric Processes and Their Role in Climate (SPARC), The Role of Halogen Chemistry in Polar Stratospheric Ozone Depletion: Report from the June 2008 Cambridge, U.K. Workshop for an Initiative under the Stratospheric Processes and Their Role in Climate (SPARC) Project of the World Climate Research Programme*, available at http://www.atmosp.physics.utoronto.ca/SPARC/HalogenChem_Final_20090213.pdf, **2009**.

(12) Papanastasiou, D. K.; Burkholder, J. B. In preparation.

(13) DeMore, W. B.; Tschuikow-Roux, E. *J. Phys. Chem.* **1990**, *94*, 5856.

(14) von Hobe, M.; Stroh, F.; Beckers, H.; Benter, T.; Willner, H. *Phys. Chem. Chem. Phys.* **2009**, *11*, 1571.

(15) Cox, R. A.; Hayman, G. D. *Nature* **1988**, *332*, 796.

(16) Huder, K. J.; DeMore, W. B. *J. Phys. Chem.* **1995**, *99*, 3905.

(17) Bloss, W. J.; Nickolaisen, S. L.; Salawitch, R. J.; Friedl, R. R.; Sander, S. P. *J. Phys. Chem. A* **2001**, *105*, 11226.

(18) Moore, T. A.; Okumura, M.; Seale, J. W.; Minton, T. K. *J. Phys. Chem. A* **1999**, *103*, 1691.

(19) Chen, H.-Y.; Lien, C.-Y.; Lin, W.-Y.; Lee, Y. T.; Lin, J. J. *Science* **2009**, *324*, 781.

(20) Ammann, M.; Atkinson, R.; Cox, R. A.; Crowley, J.; Hynes, R.; Jenkin, M. E.; Mellouki, W.; Rossi, M. J.; Troe, J.; Wallington, T. International Union of Pure and Applied Chemistry http://www.iupac-kinetic.ch.cam.ac.uk/index.html, 2008.

(21) Madronich, S. Tropospheric Ultraviolet and Visible (TUV) Radiation Model; http://cprm.acd.ucar.edu/Models/TUV/, 2009.

(22) Kawa, S. R.; Stolarski, R. S.; Newman, P. A.; Douglass, A. R.; Rex, M.; Hofmann, D. J.; Santee, M. L.; Frieler, K. *Atmos. Chem. Phys. Discuss.* **2009**, *9*, 13327.

(23) von Hobe, M.; Salawitch, R. J.; Canty, T.; Keller-Rudek, H.; Moortgat, G. K.; Grooss, J.-U.; Müller, R.; Stroh, F. *Atmos. Chem. Phys.* **2007**, *7*, 3055.

(24) Basco, N.; Hunt, J. E. *Int. J. Chem. Kinet.* **1979**, *11*, 649.

JP9065345